Evidence for multiple, distinct ADAR-containing complexes in *Xenopus laevis*

CATERINA T.H. SCHWEIDENBACK,[1,2] AMY B. EMERMAN,[1,2] ASHWINI JAMBHEKAR,[1,2] and MICHAEL D. BLOWER[1,2]

[1]Department of Molecular Biology, Massachusetts General Hospital, Boston, Massachusetts 02114, USA
[2]Department of Genetics, Harvard Medical School, Boston, Massachusetts 02115, USA

ABSTRACT

ADAR (adenosine deaminase acting on RNA) is an RNA-editing enzyme present in most metazoans that converts adenosines in double-stranded RNA targets into inosines. Although the RNA targets of ADAR-mediated editing have been extensively cataloged, our understanding of the cellular function of such editing remains incomplete. We report that long, double-stranded RNA added to *Xenopus laevis* egg extract is incorporated into an ADAR-containing complex whose protein components resemble those of stress granules. This complex localizes to microtubules, as assayed by accumulation on meiotic spindles. We observe that the length of a double-stranded RNA influences its incorporation into the microtubule-localized complex. ADAR forms a similar complex with endogenous RNA, but the endogenous complex fails to localize to microtubules. In addition, we characterize the endogenous, ADAR-associated RNAs and discover that they are enriched for transcripts encoding transcriptional regulators, zinc-finger proteins, and components of the secretory pathway. Interestingly, association with ADAR correlates with previously reported translational repression in early embryonic development. This work demonstrates that ADAR is a component of two, distinct ribonucleoprotein complexes that contain different types of RNAs and exhibit diverse cellular localization patterns. Our findings offer new insight into the potential cellular functions of ADAR.

Keywords: A-to-I editing; RNA editing; dsRNA; RNP

INTRODUCTION

Following transcription, most eukaryotic RNAs undergo some form of covalent modification. For example, mRNAs are generally spliced, capped, and polyadenylated, and ribosomal RNAs are methylated, pseudo-uridylated and cleaved (Gerbi and Borovjagin 2000). In addition, some RNAs are enzymatically edited at particular bases, resulting in precise changes to their primary sequences (Knoop 2011). The most common type of RNA editing in animals is A-to-I editing, in which an adenosine is deaminated, giving rise to an inosine (Bass 2002; Nishikura 2010). As inosine base pairs with cytidine, it is effectively recognized as guanosine by the translation and reverse-transcription machinery. Therefore, A-to-I editing is typically observed as an A-to-G transition. A-to-I editing is believed to occur in all metazoans and is highly prevalent in the human transcriptome (Wulff et al. 2011; Li and Church 2013). One study identified over 20,000 A-to-I editing sites in the transcriptome of a human lymphoblastoid cell line (Peng et al. 2012), and another study reported evidence of A-to-I editing in transcripts from more than half of human genes (Bazak et al. 2014).

The phenomenon of A-to-I editing was first discovered in *Xenopus laevis* (Bass and Weintraub 1987, 1988; Wagner and Nishikura 1988) and is mediated by the protein Adenosine Deaminase Acting on RNA (ADAR). ADAR is a double-stranded RNA (dsRNA) binding protein, and A-to-I editing is targeted to regions of dsRNA formed by either intramolecular or intermolecular base-pairing (Bass 2002; Nishikura 2010). Although there exists a single *Xenopus* ADAR, mammals have two catalytically active ADARs, ADAR1 and ADAR2, and both are essential in mice (Higuchi et al. 2000; Wang et al. 2004; Nishikura 2010). In humans, mutations in ADAR1 are associated with two diseases, dyschromatosis symmetrica hereditaria and Aicardi-Goutieres syndrome, and misregulation of ADAR1 has been implicated in hepatocellular carcinoma (Miyamura et al. 2003; Rice et al. 2012; Chen et al. 2013; Slotkin and Nishikura 2013).

Since the initial discovery of A-to-I editing, tremendous progress has been made characterizing the biochemical and enzymatic properties of ADAR. Nevertheless, several pieces

Corresponding author: blower@molbio.mgh.harvard.edu
Article published online ahead of print. Article and publication date are at http://www.rnajournal.org/cgi/doi/10.1261/rna.047787.114.

of evidence indicate that our understanding of the cellular function of A-to-I editing is incomplete. The most well-studied role of ADAR is to alter the coding potential of particular mRNAs, either by targeting specific adenosines in exons, yielding point mutations, or by targeting splice sites, resulting in alternatively spliced transcripts (Bass 2002; Nishikura 2010). However, the vast majority of editing events in humans occur in the 5′ and 3′ untranslated regions (UTRs) and introns of mRNAs and, therefore, do not modify the target RNA's coding potential (Athanasiadis et al. 2004; Hundley and Bass 2010; Nishikura 2010; Park et al. 2012). One explanation is that editing in 3′ UTRs modulates microRNA (miRNA) binding sites located there. Although there is evidence that A-to-I editing affects some miRNA binding sites, the majority of editing sites in 3′ UTRs neither create nor destroy predicted miRNA binding sites (Liang and Landweber 2007; Borchert et al. 2009). Recent data indicate that the set of transcripts targeted by ADAR1 is more well conserved across different human cell types than the specific editing sites themselves (Park et al. 2012). This observation suggests that the presence of an editing event within an RNA is more important than the precise location of that event, supporting the hypothesis that editing has a function beyond recoding RNAs. Furthermore, it is unlikely that ADAR evolved primarily to diversify the coding potential of mRNAs as most editing in human coding sequences does not confer an adaptive advantage (Xu and Zhang 2014). Rather, it is postulated that ADAR had an unknown ancestral function and later evolved to target the codons of particular transcripts (Bass 2002; Gray 2012; Xu and Zhang 2014). Although a few studies have reported specific roles for A-to-I editing beyond recoding, including influencing RNA stability (Scadden and Smith 1997; Scadden 2005) and driving nuclear localization (Zhang and Carmichael 2001), these roles have not proven widely generalizable (Hundley and Bass 2010; Nishikura 2010). Therefore, the fundamental function of the vast majority of ADAR-mediated editing events remains undetermined.

We initially embarked on the experiments described herein with the goal of characterizing RNA motifs involved in RNA localization. Specifically, we sought to uncover the sequence and structural motifs responsible for mRNA localization to spindle microtubules, a phenomenon that has been observed in a wide variety of organisms (Raff et al. 1990; Groisman et al. 2000; Lambert and Nagy 2002; Blower et al. 2007; Kingsley et al. 2007; Lécuyer et al. 2007; Eliscovich et al. 2008; Rabinowitz and Lambert 2010; Sharp et al. 2011). In the course of our investigations, we made the interesting observation that long, dsRNA added exogenously to *X. laevis* egg extract localizes to spindle microtubules.

Here, we report that exogenous dsRNA is incorporated into a microtubule-localized ribonucleoprotein complex in *X. laevis* egg extract. This complex contains ADAR as well as several proteins with established roles in RNA storage and localization. In the absence of exogenous dsRNA, we find that ADAR exists in a similar complex with endogenous mRNAs. The endogenous complex contains many of the same proteins as the exogenous dsRNA complex but fails to localize to spindle microtubules. Our experiments reveal that the length of double-strandedness in a substrate RNA is one factor that affects whether or not the ADAR–RNA complex will localize to spindle microtubules. Taken together, these results provide insight into the possible roles of ADAR-mediated RNA editing beyond recoding genes.

RESULTS

Exogenous double-stranded RNA localizes to spindle microtubules

A growing body of research demonstrates that specific messenger RNAs (mRNAs) localize to spindle microtubules in snail, fly, frog, and human cells (Raff et al. 1990; Groisman et al. 2000; Lambert and Nagy 2002; Blower et al. 2007; Kingsley et al. 2007; Lécuyer et al. 2007; Eliscovich et al. 2008; Rabinowitz and Lambert 2010; Sharp et al. 2011). We aimed to identify the *cis*-acting RNA sequence and structural motifs that specify localization of the spindle-enriched RNAs, using a cell-free extract derived from *X. laevis* eggs as a model system. *Xenopus* eggs are arrested in metaphase of meiosis II, and the extract produced from these eggs forms meiotic spindles around exogenously added *Xenopus* sperm chromatin (Hannak and Heald 2006). To test the localization of a particular RNA to these egg-extract spindles, the RNA is transcribed in vitro with a fluorescent label, added to the egg extract, and assayed for recruitment to the spindles using fluorescence microscopy (Blower et al. 2007). Using this system, we began to parse the sequence and structural elements governing RNA localization to spindle microtubules.

While investigating the role of RNA secondary structure in spindle localization, we made an interesting and unexpected discovery: long, exogenous dsRNA localizes robustly to *Xenopus* meiotic spindles. For three unrelated RNAs, we observe that neither the sense nor the antisense strands alone localize to spindle microtubules, whereas if the two strands are annealed, the resulting dsRNA accumulates at the poles of the meiotic spindles (Fig. 1A). As the three RNAs tested share no detectable homology, spindle localization appears to be independent of primary sequence. Of note, double-stranded structures in the 3′ UTR of the *Drosophila* bicoid mRNA are required for the mRNA's localization to spindle microtubules in syncytial embryos and to the oocyte anterior (Macdonald and Struhl 1988; MacDonald 1990; Ferrandon et al. 1994, 1997).

In many systems, dsRNA is either processed via the RNA interference (RNAi) pathway into small interfering RNAs (siRNAs) or triggers an antiviral response by activating protein kinase R (PKR). It has been shown that *Xenopus* early embryos lack Ago2 endonuclease activity, required for RNAi (Lund et al. 2011). Furthermore, addition of double-stranded siRNAs to *Xenopus* early embryos saturates a limited supply of maternal Ago protein, resulting in impaired miRNA

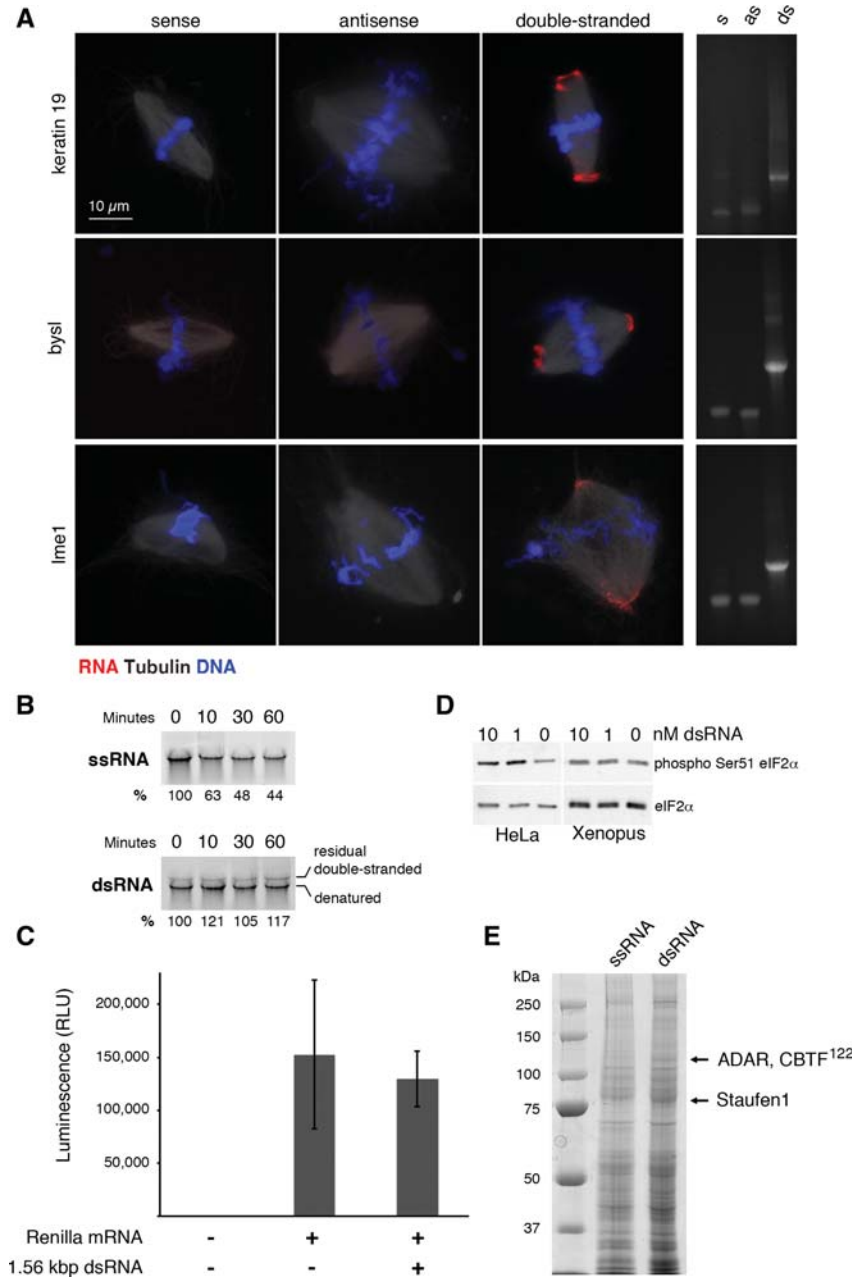

FIGURE 1. Fate of exogenous dsRNA added to *Xenopus* egg extract. (*A*) Fluorescence imaging of Cy3-labeled RNA (red) added to egg-extract spindles at a final concentration of 12.5 nM. DNA (blue) is stained with DAPI, and microtubules (white) are visualized by the addition of HiLyte Fluor 488-tubulin. Single-stranded RNAs correspond to the sense or antisense strand of a 1.56 kb fragment from the *X. laevis* keratin-19 cDNA, a 1.75 kb fragment from the *X. laevis* bysl cDNA, or a 1.5 kb fragment from the *Saccharomyces cerevisiae* IME1 promotor. Double-stranded RNAs were formed by annealing the sense and antisense transcripts prior to addition to egg extract. For all three dsRNAs, the average percentage of spindles exhibiting RNA-localization from three biological replicates was >90%. Scale bar is 10 μm. Native agarose gels of the sense (s), antisense (as), and double-stranded (ds) RNAs stained with ethidium bromide are presented to the right of the images. (*B*) Time course of the stability of single- and double-stranded keratin-19 RNA in egg extract. Percent of RNA remaining is relative to 0 min. (*C*) Luciferase assay performed in egg extract with or without 1.56 kbp double-stranded keratin-19 RNA added at 12.5 nM. (*D*) Western blots for eIF2α and phosphorylated eIF2α in HeLa cell extract and *Xenopus* egg extract with or without added dsRNA. (*E*) SDS-PAGE of egg-extract proteins that coprecipitate with exogenous single- or double-stranded keratin-19 RNA coupled to magnetic beads. Arrows indicate two bands that reproducibly coprecipitate only with dsRNA. The most abundant components of these bands, as determined by mass spectrometry, are listed.

processing by Dicer (Lund et al. 2011). Consistent with these reports, we find that exogenous dsRNA is not processed by Dicer, as it remains stable in *Xenopus* egg extract (Fig. 1B). We also tested whether exogenous dsRNA added to *Xenopus* egg extract activates PKR, an antiviral response factor that binds to and is activated by dsRNA (Donnelly et al. 2013). Activated PKR phosphorylates the translation initiation factor eIF2α leading to global translational repression (Donnelly et al. 2013). Using a luciferase reporter assay, we find that addition of exogenous dsRNA does not significantly repress translation of the reporter (Fig. 1C). Furthermore, we observe that phosphorylated eIF2α levels do not change in egg extract in response to added dsRNA (Fig. 1D). In contrast, phosphorylated eIF2α increases in HeLa cell extract following the addition of dsRNA (Fig. 1D). Thus, we conclude that exogenous dsRNA does not activate the PKR response in *Xenopus* egg extract. The absence of a PKR response has also been noted in mouse oocytes (Wianny and Zernicka-Goetz 2000; Stein et al. 2005) and undifferentiated embryonic stem cells (Yang et al. 2001). Therefore, in *X. laevis* eggs, long, exogenous dsRNA is not a substrate for either of the two most well-studied dsRNA-activated pathways: RNAi and the PKR response.

An ADAR-containing complex is necessary for spindle localization of dsRNA

To identify factors that mediate localization of exogenous dsRNA to meiotic spindles, we performed a biochemical screen for proteins in the egg extract that bind dsRNA but not ssRNA. To this end, we coupled biotinylated RNA to streptavidin beads, incubated the beads in egg extract, and purified bound proteins. We analyzed the eluted proteins by SDS-PAGE and detected two bands that reproducibly copurify with dsRNA-coupled beads but not with ssRNA-coupled beads (Fig. 1E). Using tandem mass spectrometry, the main component of the first band was identified as ADAR. This band also contains CBTF^{122}/ILF3/NF90,

a protein known to associate with translationally inactive mRNAs in early *Xenopus* embryos (Brzostowski et al. 2000). The main component of the second band was identified as Staufen1, a protein with an established role in RNA localization in several organisms, including *X. laevis* (Yoon and Mowry 2004; Jansen and Niessing 2012). ADAR, Staufen1, and CBTF[122] all contain canonical dsRNA binding domains.

To test if either of our two primary candidates, ADAR or Staufen1, is necessary for dsRNA localization to spindle microtubules, we generated antibodies to each and used these antibodies to immunodeplete the proteins from egg extract. We were able to deplete ~75% of Staufen1 and ~90% of ADAR (Fig. 2A). We find that depletion of Staufen1 has no effect on the localization of dsRNA to spindles, whereas depletion of ADAR completely abrogates localization (Fig. 2B). Depleting ADAR does not affect spindle morphology (Fig. 2B) nor does it result in dramatic destabilization of the dsRNA, as the dsRNA remains as stable as ssRNA in undepleted egg extract (Figs. 1B, 2C).

To determine whether the exogenous dsRNA undergoes A-to-I editing in *Xenopus* egg extract, we reverse transcribed and sequenced the exogenous transcripts following their incubation in egg extract or ADAR-depleted egg extract (Fig. 2D). We observe significant editing of the transcripts incubated in nondepleted egg extract. On average, ~16% of adenosines are changed to guanosines in the sequenced cDNA (Fig. 2D). In contrast, transcripts incubated in ADAR-depleted egg extract exhibit A-to-I editing at <0.1% of the adenosines (Fig. 2D), indicating that editing of the exogenous dsRNA is due to ADAR. We were able to rescue editing in ADAR-depleted extract with the addition of recombinant *X. laevis* ADAR purified from insect cells (Fig. 2D,E). Following rescue, ~30% of the adenosines within the exogenous dsRNA are edited (Fig. 2D).

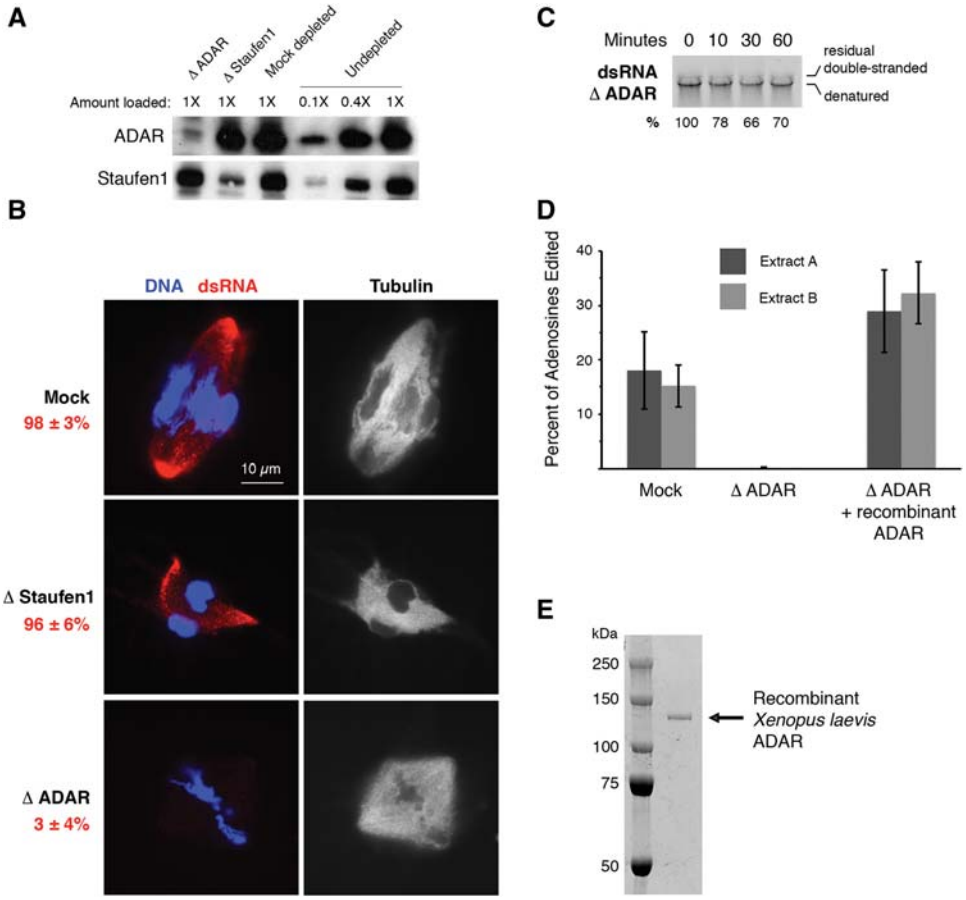

FIGURE 2. Requirement of an ADAR-containing complex for the spindle localization of dsRNA. (*A*) Western blot demonstrating immunodepletion of ~90% of ADAR and ~75% of Staufen1 from egg extract. (*B*) Fluorescence imaging of dsRNA localization to spindle poles in mock, Staufen1, or ADAR-depleted egg extract. The average percentage of spindles exhibiting localized RNA from three biological replicates is reported in red text. Double-stranded keratin-19 RNA (red) is labeled with Cy3-CTP, DNA (blue) is stained with DAPI, and microtubules (white) are visualized by the addition of HiLyte Fluor 488-tubulin. Scale bar is 10 μm. (*C*) Time course of dsRNA stability in ADAR-depleted egg extract. Percent of double-stranded keratin-19 RNA remaining is relative to 0 min. (*D*) Quantification of the average percentage of adenosines edited within a 300 base region on one strand of double-stranded IME1 RNA incubated for 40 min in egg extract. Experiment was performed in mock-depleted egg extract, ADAR-depleted egg extract, and ADAR-depleted egg extract rescued with 1 μM purified recombinant ADAR. (*E*) Coomassie-stained polyacrylamide gel of purified recombinant *X. laevis* ADAR.

Despite the ability of recombinant ADAR to rescue A-to-I editing of the exogenous dsRNA, it does not rescue the spindle-localization defect (data not shown). Therefore, editing alone is not sufficient to mediate localization of the dsRNA. We hypothesize that the inability to rescue localization with recombinant ADAR is either due to the codepletion of necessary factors that complex with ADAR or to the absence of proper protein modifications on recombinant ADAR (Desterro et al. 2005; Macbeth et al. 2005) that are required for the protein's microtubule-localization function.

Spindle-localized, exogenous dsRNA exists in ribonucleoprotein complexes with canonical RNA regulating proteins

Well-studied, localized RNAs in many organisms are known to exist in large ribonucleoprotein (RNP) complexes that are necessary for the transport or anchoring of the localized RNA (St Johnston 2005). As we observe that exogenous dsRNA added to frog egg extract localizes to granule-like structures on spindle microtubules (Figs. 1A, 2B), we investigated whether candidate proteins colocalize with the dsRNA using immunocytochemistry. We find that ADAR, Staufen1, and CBTF^{122} exhibit remarkable colocalization with the exogenous dsRNA (Fig. 3A). Next, we tested whether several RNA-binding proteins with known roles in RNA regulation also colocalize with the dsRNA. We observe colocalization with Vera/Vg1 RBP, a protein implicated in localizing mRNAs to the vegetal cortex of *Xenopus* oocytes (Mowry 1996; Deshler et al. 1997), Xp54/Dhh1/RCK, an RNA helicase found in multiple types of RNA granules (including P-bodies and stress granules) in many organisms (Ladomery et al. 1997; Thomas et al. 2011), and the 40S ribosomal protein S6, an established component of stress granules (Fig. 3A; Thomas et al. 2011). In contrast, we do not detect convincing colocalization between the exogenous dsRNA and Xiwi, a *Xenopus* Piwi protein (Fig. 3A; Lau et al. 2009). Furthermore, despite accumulation of the dsRNA at spindle poles in a manner suggestive of minus-end-directed, motor-driven transport, we were unable to detect consistent colocalization with the minus-end-directed motors dynein or XCTK2/Kinesin-14 (data not shown). These data demonstrate that exogenous dsRNA is present in an RNP containing proteins with established roles in RNA regulation.

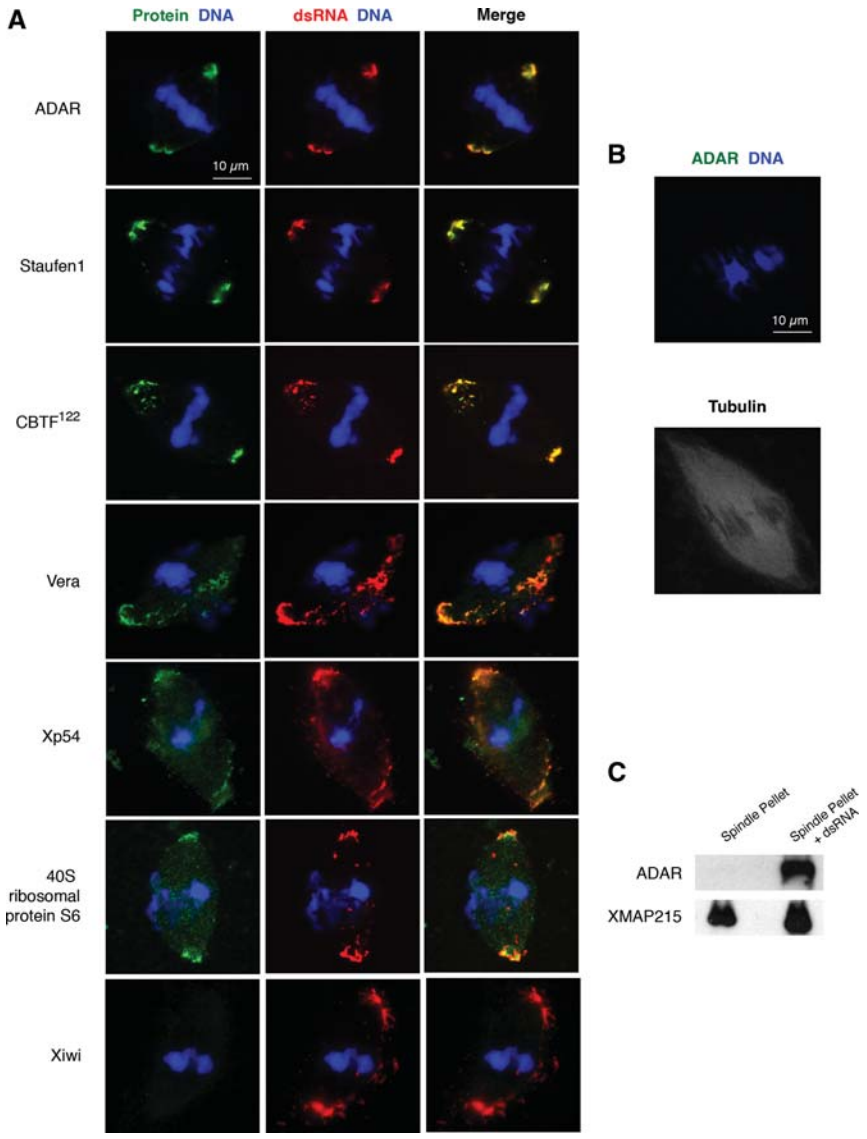

FIGURE 3. Characterization of the spindle-localized dsRNA complex. (*A*) Immunofluorescence imaging of candidate RNA-interacting proteins (green) on spindles with localized, exogenous dsRNA (red). Double-stranded keratin-19 RNA is labeled with Cy3-CTP, DNA (blue) is stained with DAPI, and secondary antibodies are conjugated to Alexa 488. Scale bar is 10 μm. (*B*) ADAR staining (green) on spindles in the absence of exogenous dsRNA. DNA (blue) is stained with DAPI, secondary antibody is conjugated to Alexa 488, and microtubules (second panel, white) are visualized by the addition of rhodamine-tubulin. Scale bar is 10 μm. (*C*) Western blots on pelleted spindles isolated from egg extract with or without exogenous double-stranded kertain-19 RNA. XMAP215, a microtubule-binding protein, serves as a loading control.

To determine whether exogenous dsRNA induces the formation of RNPs that accumulate on spindle microtubules or whether the exogenous dsRNA is recruited to an existing granule, we stained spindles for the same proteins in the absence of exogenous dsRNA. We were not able to detect spindle accumulation of any of the factors that colocalize with exogenous dsRNA in its absence (Fig. 3B and data not shown).

It remains possible that endogenous complexes exist but are too sparse to detect by immunofluorescence. As a complementary experiment, we pelleted spindles from egg extract with or without exogenous dsRNA and analyzed the amount of ADAR that copellets by Western blot. ADAR is highly enriched on spindles pelleted from egg extract containing exogenous dsRNA, whereas XMAP 215, a microtubule-binding protein, is equally abundant on spindles from extract with or without dsRNA (Fig. 3C). Together, these results indicate that exogenous dsRNA drives accumulation of ADAR-containing RNPs on spindle microtubules. However, we cannot rule out the possibility that a similar endogenous complex exists whose abundance is below our detection threshold.

ADAR associates with endogenous *Xenopus* mRNAs

Our results demonstrate that long, exogenous dsRNA is bound to and edited by ADAR in *Xenopus* egg extract, leading us to question if ADAR binds endogenous mRNAs. To identify potential endogenous ADAR substrates, we immunoprecipitated ADAR from egg extract and isolated coprecipitating RNAs (Fig. 4A). The mass of RNA that coprecipitates with ADAR is 13.6-fold larger than the mass of RNA recovered from a mock immunoprecipitation using nonspecific rabbit IgG (Fig. 4A). We sequenced the ADAR-associated RNAs and calculated an ADAR-enrichment value for each transcript that was defined as the normalized abundance of the transcript in the ADAR precipitation divided by the normalized abundance of the transcript in total egg extract. A plot of transcript density as a function of the $\log_2$ (ADAR enrichment) deviates from a normal curve, demonstrating a shoulder of transcripts with high ADAR enrichments (Fig. 4B). We verified that transcripts predicted to be highly ADAR-enriched based on our sequencing data were also enriched in ADAR precipitations from multiple extracts as measured by RT-PCR (Fig. 4C and data not shown).

As ADAR targets double-stranded RNA, often formed via intramolecular base-pairing (Bass 2002; Nishikura 2010), we investigated whether transcripts computationally predicted to form hairpins are more likely to coprecipitate with

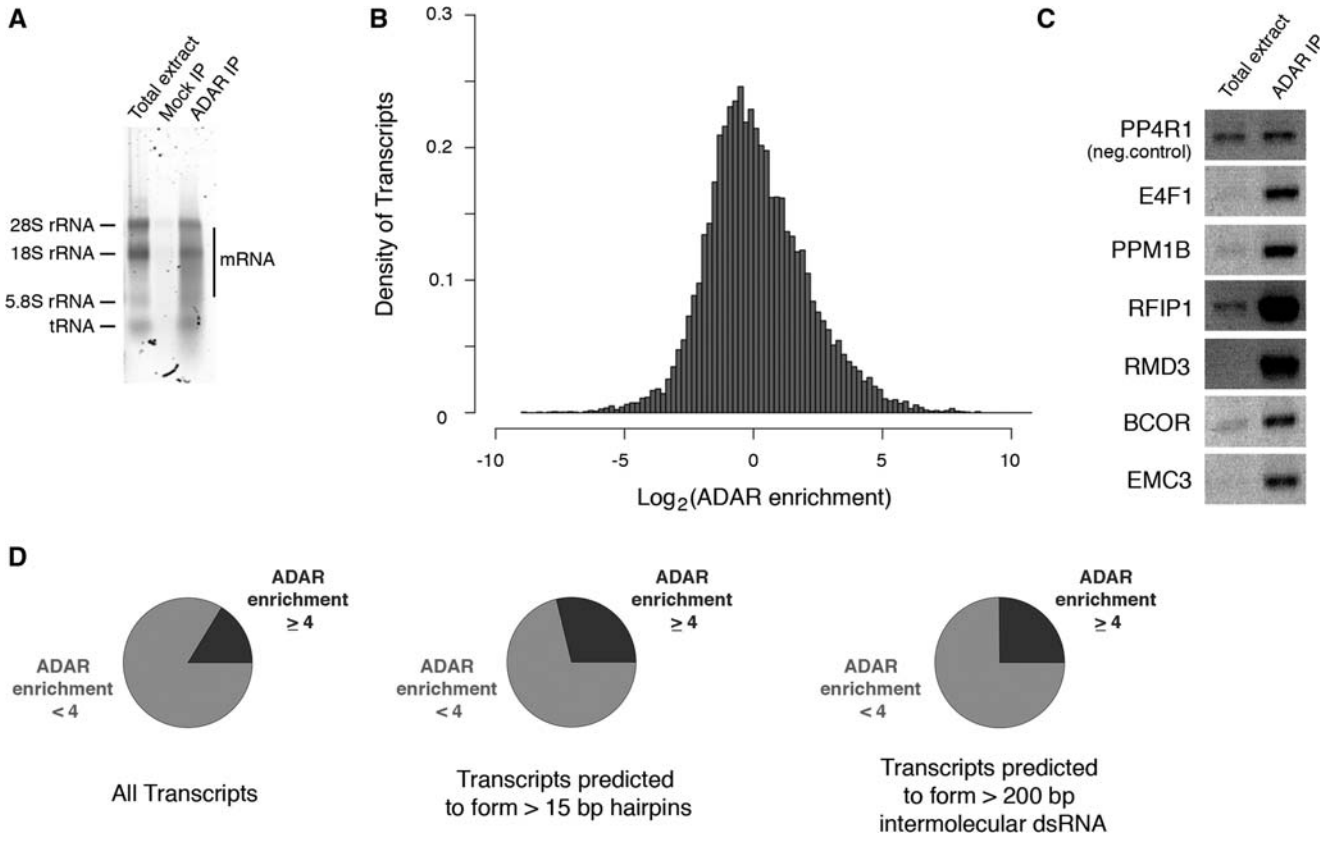

FIGURE 4. Isolation of endogenous ADAR-associated RNAs. (*A*) Agarose gel of RNA isolated from total egg extract, mock immunoprecipitation or ADAR immunoprecipitation. (*B*) Histogram of transcript density as a function of ADAR enrichment. (*C*) RT-PCR for predicted ADAR-enriched transcripts from total egg extract or an ADAR immunoprecipitation. PP4R1, a transcript predicted not to be ADAR-enriched, serves as a negative control. Results shown are from one representative experiment. Similar results were obtained from a total of three biological replicates. (*D*) Charts representing the fraction of total transcripts, transcripts predicted to form >15 bp hairpins, and transcripts predicted to form >200-bp intermolecular dsRNA that have ADAR-enrichment values ≥4. *P*-value for overrepresentation of ADAR-enriched transcripts among transcripts predicted to form hairpins is 1×10^{-14} using a one-sided Fisher's exact test. *P*-value for overrepresentation of ADAR-enriched transcripts among transcripts predicted to form intermolecular dsRNA is $<2.2 \times 10^{-16}$ using a one-sided Fisher's exact test.

ADAR. We identified those transcripts in the *X. laevis* transcriptome predicted to form >15 bp hairpin structures, which together represent ~5% of all transcripts (Supplemental Table 1). Given the difficulty of predicting complex secondary and tertiary RNA structures that might confer ADAR specificity (Rieder et al. 2013), the actual percentage of transcripts with potential ADAR target sites is likely much higher. We find that while 16% of all transcripts have ADAR-enrichment values ≥4, 29% of transcripts predicted to form >15 bp hairpins are at least fourfold ADAR-enriched ($P = 1 \times 10^{-14}$ using one-sided Fisher's exact test) (Fig. 4D). Thus, transcripts predicted to form hairpins are more likely to coprecipitate with ADAR.

RNA hairpins can arise from pairing between inverted copies of a repetitive element present within an mRNA. In humans, intramolecular dsRNA formed by inverted Alu elements account for the vast majority of editing targets (Athanasiadis et al. 2004; Kim et al. 2004; Park et al. 2012). To determine if predicted hairpins in *Xenopus* mRNAs are the consequence of inverted repetitive elements, we compared predicted hairpin sequences to *Xenopus* Repbase sequences (Jurka et al. 2005). Of the sequences predicted to form intramolecular hairpins >15 bp, 16% have significant homology with repetitive sequences (Supplemental Table 1). However, none of the hairpins that match repetitive sequences contain two inverted copies of a repetitive element. Rather, the hairpins result from inherently structured sequences within a single repetitive element. Due to the incomplete nature of the *Xenopus laevis* genome, our analysis is likely an underestimate of the contribution of repetitive elements to intramolecular hairpins.

Another source of endogenous dsRNA is intermolecular dsRNA formed by base-pairing between complementary transcripts (Werner 2005). It is possible for two transcripts to exhibit extensive complementarity if they are transcribed from overlapping open reading frames located on opposite strands of the genome or if they each harbor the same repetitive element in opposite orientations. To investigate whether intermolecular dsRNA coprecipitates with ADAR, we computationally identified *X. laevis* transcripts predicted to form intermolecular dsRNA longer than 200 bp. The identified transcripts represent ~15% of the transcriptome (Supplemental Table 1). We observe that 25% of the transcripts predicted to form >200-bp intermolecular dsRNA have ADAR-enrichment values ≥4, whereas only 16% of all transcripts are similarly ADAR-enriched ($P < 2.2 \times 10^{-16}$ using one-sided Fisher's exact test) (Fig. 4D). Therefore, transcripts with the potential to form long, intermolecular dsRNA are more likely to coprecipitate with ADAR. Furthermore, of the transcripts predicted to form intermolecular dsRNA >200 bp, 17% were homologous to repetitive elements, suggesting that repetitive elements may play a role in promoting intermolecular base-pairing (Supplemental Table 1).

It would be interesting to investigate whether ADAR-associated RNAs are enriched for transcripts predicted to undergo A-to-I editing. Unfortunately, only a small number of *Xenopus* editing sites have been cataloged to date (Kimelman and Kirschner 1989; Saccomanno and Bass 1999; Zaranek et al. 2010). Moreover, owing to the lack of a completed genome and the absence of a database of polymorphisms for *X. laevis*, genome-wide identification of RNA editing sites is not currently feasible.

To investigate whether the endogenous RNA targets of ADAR are enriched for transcripts encoding proteins with particular cellular functions, we performed gene ontology analysis (Huang da et al. 2009a,b) on total and ADAR-enriched *Xenopus* transcripts. We find that the ADAR-associated mRNAs are enriched for transcripts encoding transcriptional regulators, zinc-finger proteins, and components of the secretory pathway (Supplemental Table 2). It has been demonstrated that editing targets in human B cells are also enriched for mRNAs encoding zinc-finger proteins (Wang et al. 2013), suggesting that ADAR plays a conserved role in regulating this class of mRNAs. The finding that ADAR-associated mRNAs tend to encode transcription factors and proteins involved in signal transduction led us to hypothesize that ADAR might sequester and translationally repress maternal transcripts needed later in development. To test if ADAR-associated transcripts tend to be translationally repressed, we took advantage of recently published data (Subtelny et al. 2014) using ribosome profiling (Ingolia et al. 2009) to measure the translational efficiencies of mRNAs from *X. laevis* embryos. ADAR-enriched transcripts tend to have lower translational efficiencies than total transcripts in 4–8 cell (stage 3–4) embryos; the mean of the $\log_2$ translational efficiency of all transcripts is −0.126, whereas the mean of the $\log_2$ translational efficiency for ADAR-associated transcripts is −0.707 ($P = 1 \times 10^{-7}$, unpaired *t*-test) (Fig. 5A; Supplemental Table 3). However, the same effect is not observed in later embryos (Fig. 5B). In post-gastrulation (stage 12–12.5) embryos, the mean of the $\log_2$ translational efficiency of all transcripts is −0.448, whereas the mean of the $\log_2$ translational efficiency for ADAR-associated transcripts is −0.163 ($P = 3 \times 10^{-3}$, unpaired *t*-test) (Fig. 5B). These results suggest that ADAR might play a role in translational repression during early *Xenopus* embryogenesis.

ADAR-RNPs containing endogenous mRNAs share many protein components with ADAR-RNPs containing exogenous dsRNA but are functionally distinct

In light of ADAR's interaction with endogenous RNAs, we examined whether the ADAR complex containing endogenous RNAs (ADAR-endoRNP) is biochemically similar to the ADAR complex containing long, exogenous dsRNA (ADAR-exoRNP). As we do not detect an accumulation of ADAR at spindle poles in the absence of added dsRNA, we could not investigate the protein composition of the ADAR-endoRNPs by staining and imaging meiotic spindles,

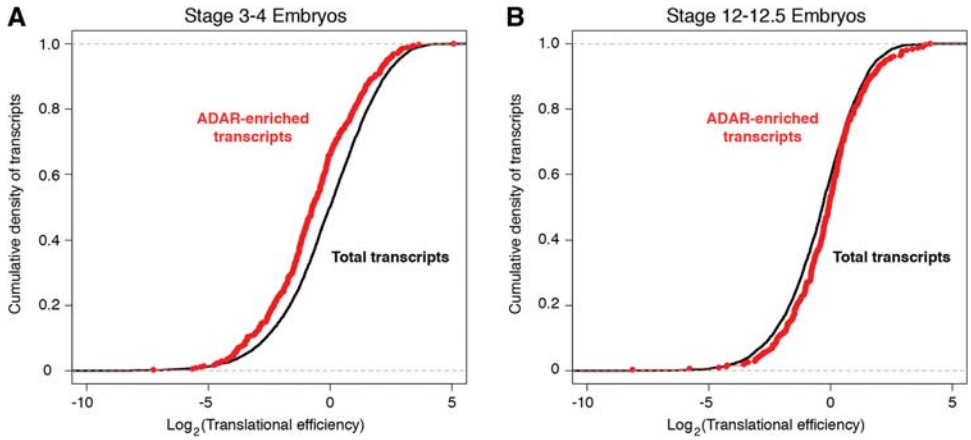

FIGURE 5. Translational efficiency of ADAR-associated transcripts. (*A*) Plot of the cumulative density of transcripts as a function of translational efficiency in stage 3–4 *X. laevis* embryos. Translational efficiency values are based on published data (Subtelny et al. 2014). Black line represents all abundant transcripts for which translational efficiency data were available (~4500 transcripts). Red line represents the subset of those transcripts with ADAR-enrichment values ≥4. (*B*) Same as *A*, but for stage 12–12.5 embryos.

as we did for the ADAR-exoRNPs. Instead, we chose a biochemical approach and immunoprecipitated ADAR from *Xenopus* egg extract without exogenous dsRNA. We isolated proteins that coprecipitate with ADAR (but not with nonspecific IgG) and identified them by tandem mass spectrometry. Our results reveal that several components of ADAR-exoRNPs are also components of ADAR-endoRNPs, including ADAR, Staufen1, CBTF[122], Vera, and Xp54 (Fig. 6A). In addition, we identified two other components of ADAR-endoRNPs: Frgy2 (Ranjan et al. 1993; Capshew et al. 2012) and RAP55/Car-1 (Tanaka et al. 2006), both of which associate with translationally repressed mRNAs in *Xenopus* oocytes,

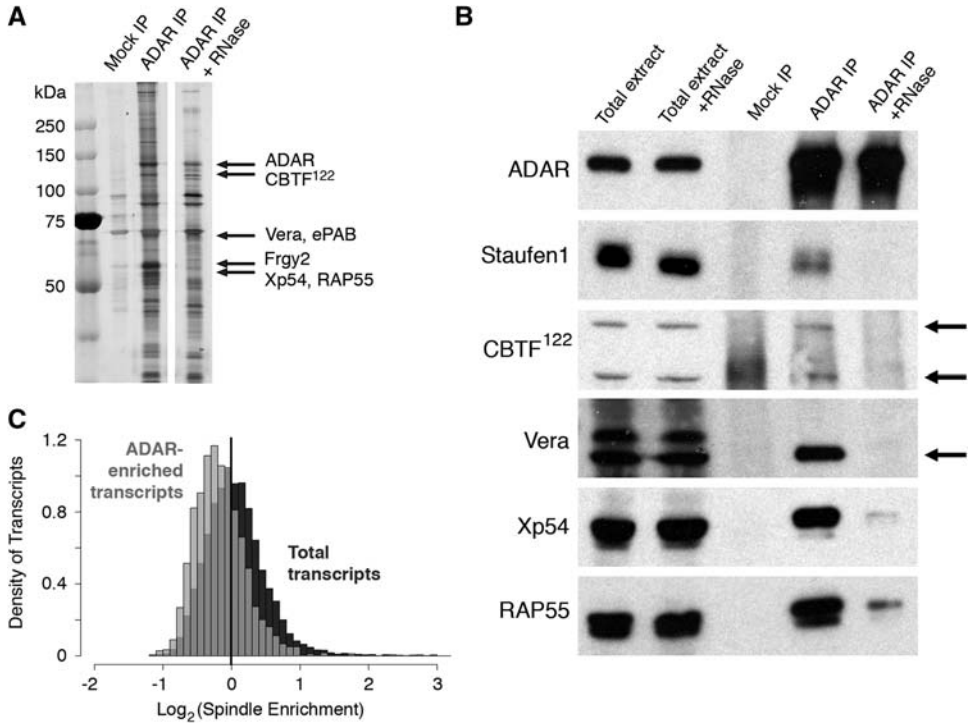

FIGURE 6. Characterization of endogenous ADAR-RNPs. (*A*) SDS-PAGE of proteins that coimmunoprecipitate with ADAR from egg extract or egg extract treated with RNaseA. The precipitations were washed with buffer containing 1% Triton prior to elution with SDS. The most abundant components of bands analyzed by mass spectrometry are indicated with labeled arrows. (*B*) Western blots for candidate proteins in total egg extract or ADAR-precipitations with or without RNase treatment. (*C*) Histogram of transcript density as a function of spindle-enrichment. Dark gray histogram represents all transcripts. Light gray histogram represents transcripts with ADAR-enrichment values ≥4. *P*-value for the difference in the distributions is $<3 \times 10^{-16}$ using a two-sided Mann–Whitney test with continuity correction.

and the latter of which is also a component of *P*-bodies and stress granules in human cells (Fig. 6A). These proteins fail to coprecipitate with ADAR following treatment of the egg extract with RNase (Fig. 6A), indicating that RNA is necessary for their interaction with ADAR. Western blot analysis confirms that these proteins interact with ADAR in an RNA-dependent manner (Fig. 6B). The observation that proteins known to complex with translationally silenced mRNAs in *Xenopus* oocytes are present in the ADAR-endoRNPs supports the hypothesis that these RNPs function to store and silence mRNAs during early embryogenesis.

As ADAR-endoRNPs and ADAR-exoRNPs contain many of the same protein components, and as ADAR-exoRNPs localize to the poles of spindle microtubules, we asked whether ADAR-endoRNPs also localize to spindles. Although we do not observe ADAR-endoRNPs on spindles based on ADAR staining (Fig. 6B), we investigated whether the endogenous ADAR-associated RNAs are associated with spindle microtubules. To this end, we purified meiotic spindles, isolated and sequenced copurifying RNAs, and calculated a spindle-enrichment value for each transcript (defined as the normalized abundance of the transcript in the spindle prep divided by the normalized abundance of the transcript in total egg extract) (Jambhekar et al. 2014). We then assessed whether ADAR-enriched RNAs are also spindle-enriched and find that ADAR-associated transcripts tend to be less spindle-enriched than total transcripts (Fig. 6C). The median spindle-enrichment values for all transcripts ($n = 12{,}875$) and ADAR-enriched transcripts ($n = 632$) are 1.02 and 0.87, respectively ($P < 3 \times 10^{-16}$, two-sided Mann–Whitney test) (Fig. 6C). Therefore, it appears that ADAR is a component of two similar but distinct protein complexes: one that forms on long, perfectly paired, exogenous dsRNA and localizes to spindle microtubules, and one that forms on endogenous mRNAs and is not spindle-localized. Both complexes share many proteins, but only the ADAR-exoRNPs localize to spindle microtubules.

Presumably there are some factor(s) present in the ADAR-exoRNPs that are absent in the ADAR-endoRNPs that specify localization to microtubules. In an effort to detect such factors, we compared the proteins that coprecipitate with ADAR in the presence or absence of exogenous dsRNA. We were not able to detect any candidate bands on an SDS-PAGE gel that were specific to the ADAR-exoRNPs (data not shown). This result is likely due to the fact that our anti-ADAR antibody does not precipitate ADAR-exoRNPs efficiently, as evidenced by the fact that we cannot deplete ADAR from extract already containing exogenous dsRNA (data not shown). That the ADAR-endoRNPs and ADAR-exoRNPs are differentially recognized by our anti-ADAR antibody is further evidence of structural differences between the two complexes. It is formally possible that there exists a small population of spindle-localized ADAR-endoRNPs that are poorly precipitated by our anti-ADAR antibody and whose bound RNAs we failed to identify. However, given that we can deplete ~90% of ADAR from egg extract without exogenous dsRNA, the majority of ADAR is accessible to our antibody. Furthermore, in the absence of exogenous dsRNA, we did not detect ADAR copelleting with spindles by Western blot (Fig. 3C).

Length of dsRNA influences localization to spindle microtubules

Our data raise the interesting question of which properties of an ADAR-associated RNA determine whether it is incorporated into an RNP that localizes to microtubules or one that does not. One possibility is that endogenous RNA is incorporated into a different complex than exogenous RNA. The cell might distinguish between endogenous and exogenous RNA based on proteins that are recruited to the endogenous RNA following transcription in the nucleus. Alternately, the distinct complexes might be determined by the structure of the RNA itself. Our exogenous dsRNA was perfectly base paired over its entire 1.56 kb length. In contrast, the endogenous ADAR-associated mRNAs likely have much shorter regions of complementarity. Although it would be challenging to test the role of nuclear transcription in the formation of spindle-localized ADAR-RNPs owing to a lack of transcription in *Xenopus* eggs (Newport and Kirschner 1982a,b), we can test the role of increasing lengths of double-strandedness.

To investigate whether RNAs with longer stretches of base-pairing are more likely to localize to spindle microtubules, we constructed dsRNAs in which the antisense strands base pair to all, two-thirds, or one-third of the 1.56 kb sense strand (Fig. 7A). Importantly, only the sense strand is fluorescently labeled, so that fluorescence intensity per molecule of RNA is consistent between the constructs. We tested the ability of these constructs to localize to meiotic spindles formed in *Xenopus* egg extract and found that constructs with shorter double-stranded regions localize to fewer spindles and exhibit weaker accumulation on the spindles to which they do localize (Fig. 7A). In particular, the RNA construct with a 520 nt antisense strand is not detected on spindles (Fig. 7A). To examine how length of base-pairing affects RNA interaction with ADAR, we sequenced a fraction of the RNA in each sample after incubation in egg extract but prior to spindle pelleting. The sequencing results were used to calculate the average percentage of edited adenosines on the sense strand of the 520 bp region that is double-stranded in all three dsRNA constructs (Fig. 7B). We find that all of the double-stranded constructs are edited (Fig. 7B), consistent with reports that dsRNA as short as 50 bp can undergo hyperediting by ADAR and dsRNA as short as 15 bp can be targeted for editing at specific adenosines (Nishikura et al. 1991; Polson and Bass 1994). While there is a detectable decrease in the frequency of editing on the construct with only 520 bp of dsRNA, on average 8% of the adenosines are edited, indicating that the construct does interact with ADAR even though

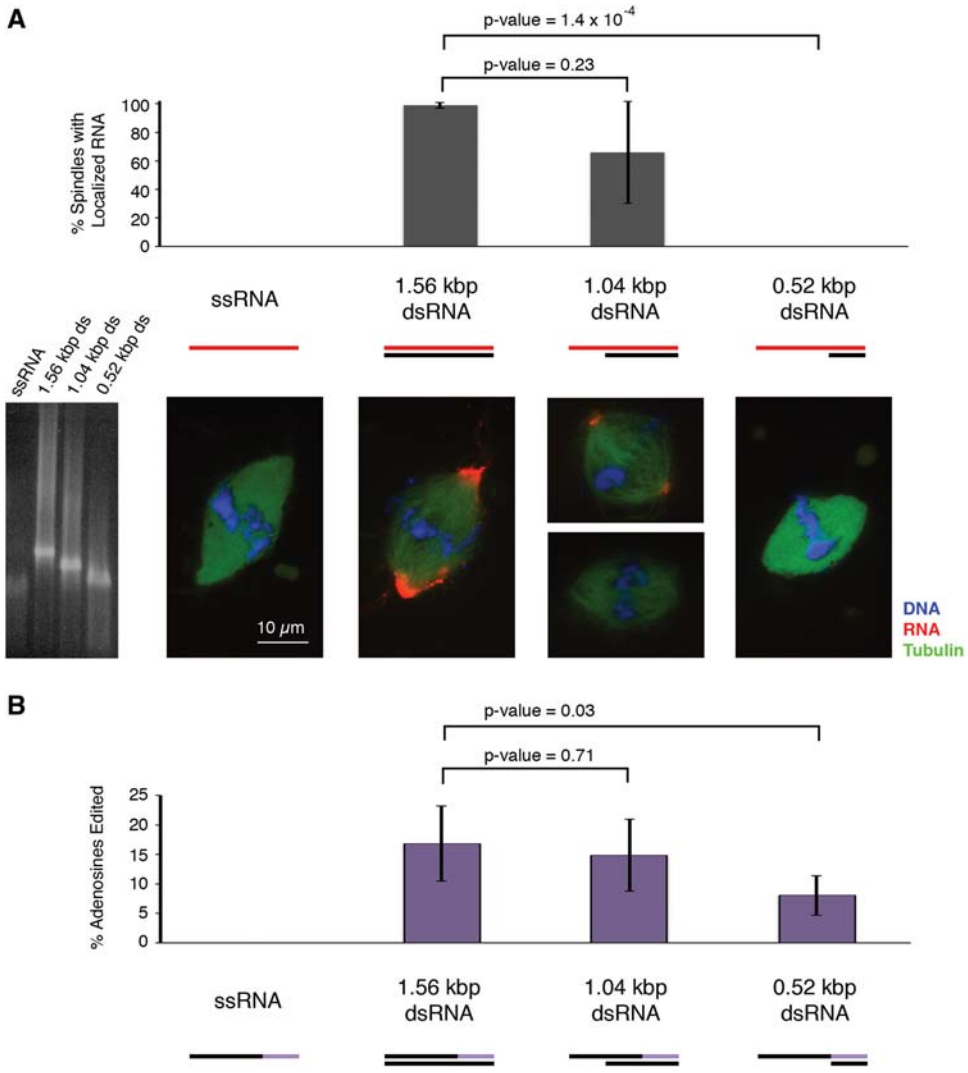

FIGURE 7. Effect of dsRNA length on spindle localization and editing. (*A*) Quantification of the percentage of spindles exhibiting localized RNA in samples containing keratin-19 RNA constructs with various lengths of double-stranded structure. Data are the average of three biological replicates. *P*-values were calculated using a two-sided paired *t*-test. *Below* the bar graph are representative images of the spindles for each RNA construct. RNA (red) is labeled with Cy3-CTP, DNA (blue) is stained with DAPI, and microtubules (green) are visualized by the addition of HiLyte Fluor 488-tubulin. Scale bar is 10 μm. A native agarose gel of the RNA constructs stained with ethidium bromide is shown. (*B*) Quantification of the percentage of adenosines edited in the RNA constructs during the experiment in *A*. Editing was assessed in the terminal third of the sense strand (depicted in purple). *P*-values were calculated using a two-sided Welch's *t*-test.

it fails to localize to spindles (Fig. 7A,B). Therefore, the constructs with long (~1.5 kbp) dsRNA tend to be incorporated into ADAR-RNPs that localize to spindle microtubules, whereas the constructs with shorter (~500 bp) dsRNA tend to interact with ADAR without localizing to spindles.

To verify that it is the length of dsRNA, and not the presence of a single-stranded overhang, that influences spindle localization, we tested localization of different length dsRNAs lacking overhangs (Fig. 8). Again, we find that shorter dsRNAs (1.04 and 0.52 kbp) are significantly compromised for spindle localization relative to a 1.56 kbp dsRNA (Fig. 8B,C). These data suggest that the length of double-stranded structure in an ADAR-associated RNA at least partially determines whether that RNA will localize to spindle microtubules.

DISCUSSION

We discover that ADAR is a novel component of two, distinct RNP complexes in *X. laevis* that we term ADAR-exoRNPs and ADAR-endoRNPs. Long, exogenous dsRNA is incorporated into ADAR-exoRNPs, and these complexes localize to spindle microtubules. Endogenous *X. laevis* mRNAs are found in ADAR-endoRNPs, which contain many of the same proteins present in ADAR-exoRNPs but do not localize to spindles. We find evidence that the length of double-

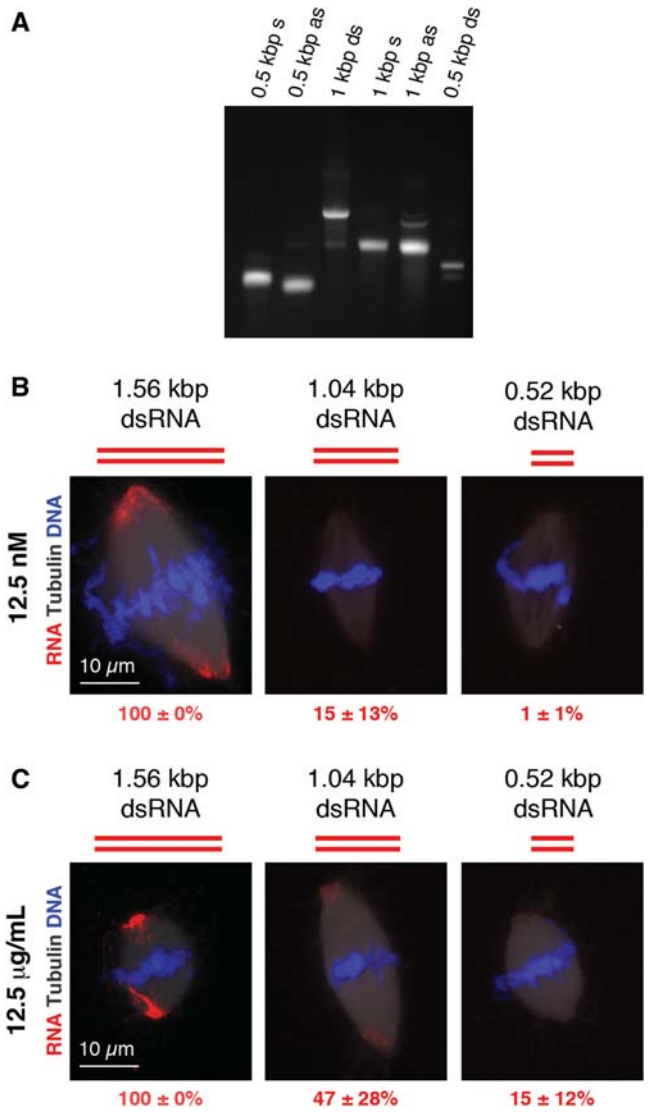

FIGURE 8. Spindle localization of dsRNAs of different lengths. (*A*) Native agarose gel of keratin-19 RNA constructs used in the experiments in *B*. Gel is stained with ethidium bromide. (*B*) Fluorescence imaging of RNA localization to spindles using dsRNAs of different lengths that do not contain single-stranded overhangs. Equivalent moles of RNA were added to each sample for a final RNA concentration of 12.5 nM. RNA (red) is labeled with Cy3-CTP, DNA (blue) is stained with DAPI, and microtubules (white) are visualized by the addition of HiLyte Fluor 488-tubulin. Scale bar is 10 μm. The average percentage of spindles exhibiting localized RNA from three biological replicates is reported in red text. (*C*) Same as in *B*, except that an equivalent mass of RNA was added to each sample for a final RNA concentration of 12.5 μg/mL.

stranded structure in an RNA is one factor influencing localization to spindle microtubules.

ADAR-exoRNPs: ADAR-RNPs containing long, exogenous dsRNA

We find that long, exogenous dsRNA localizes to the poles of meiotic spindles in *X. laevis* egg extract, and localization depends on an ADAR-containing complex. As dsRNA added exogenously to *Xenopus* egg extract is not processed by the RNAi machinery and does not activate the PKR response, this system provides a rare opportunity to study ADAR in the absence of other dsRNA-activated pathways. Insight into the cellular function of localizing exogenous dsRNA to spindle microtubules is gained from the identification of protein components of the exogenous RNA granules (ADAR-exoRNPs). In addition to ADAR, we observe that Staufen1, CBTF[122], Vera, Xp54, and ribosomal protein S6 are present in the ADAR-exoRNPs. These factors are consistent with the components of stress granules and *Xenopus* embryo storage mRNPs (Ladomery et al. 1997; Brzostowski et al. 2000; Tanaka et al. 2006; Thomas et al. 2011), both of which function to sequester and translationally silence RNAs. Interestingly, it has previously been reported that ADAR1 localizes to stress granules in human cells in response to oxidative stress or inosine-containing dsRNA (Weissbach and Scadden 2012; Ng et al. 2013). We hypothesize that the ADAR-exoRNPs are stress granule-like complexes that act to repress long, dsRNA that might arise from transposable elements or viral infection. An ADAR-mediated antiviral activity might be particularly useful in *Xenopus* oocytes as the two canonical dsRNA-activated antiviral pathways, RNA interference and the PKR response, are inactive.

Our experiments assayed localization of exogenous dsRNA to meiotic spindles as these structures constitute a dense, polarized assembly of microtubules that facilitates the detection of microtubule localization. However, it is likely that ADAR-exoRNPs localize to microtubules in general, rather than to spindle microtubules specifically. Stress granules are known to associate with microtubules, and stress granule formation is impaired following microtubule depolymerization (Bartoli et al. 2011). Therefore, the accumulation of ADAR-exoRNPs on microtubules is consistent with our model that these RNPs function as stress granule-like complexes. Nevertheless, there do exist cytoplasmic bodies that specifically localize to spindle poles. For example, aggresomes, structures that sequester aggregated, misfolded proteins, accumulate on centrosomes throughout the cell cycle (Johnston et al. 1998, 2002; Rujano et al. 2006). During cell division, localization of the aggresome to a single centrosome at one spindle pole results in asymmetric inheritance of the structure and clearing of the aggregated protein from one of the two daughter cells (Rujano et al. 2006).

ADAR-endoRNPs: ADAR-RNPs containing endogenous RNAs

We discover that endogenous ADAR-RNPs (ADAR-endoRNPs) exist and contain several of the same factors present in the ADAR-exoRNPs but do not localize to spindle microtubules. The ADAR-endoRNPs are enriched for transcripts that are predicted to form intramolecular or intermolecular double-stranded RNA, that are translationally

repressed during early development, and that encode zinc-finger transcriptional regulators. Based on these results, we hypothesize that ADAR-endoRNPs act to sequester and silence mRNAs whose protein products are needed later in development. In support of this model, we find that Frgy2, Staufen1, CBTF[122], Vera, Xp54, and RAP55/Car-1, known components of *Xenopus* embryo storage mRNPs (Ranjan et al. 1993; Ladomery et al. 1997; Brzostowski et al. 2000; Tanaka et al. 2006), are present in ADAR-exoRNPs. Of note, this is the first report of ADAR's association with these proteins. In adult worms and human cells, ADAR does not affect the translation efficiency of RNAs containing structured 3′ UTRs, suggesting that ADAR's role in translational repression might be specific to early development or to *X. laevis* early development (Hundley et al. 2008; Capshew et al. 2012). An interesting question for future studies is whether all edited RNAs are incorporated into storage mRNPs in *Xenopus* oocytes.

Most attempts to identify ADAR substrates in a wide range of organisms have relied on observing the outcome of ADAR-mediated editing: A-to-I changes between the genome and the transcriptome. Parsing the signal (i.e., true editing events) from the noise (e.g., genomic variation, sequencing errors) is challenging (Wulff et al. 2011). In addition, this method can miss ADAR targets that are hyperedited, as mapping sequencing reads from an extensively edited region of RNA to the genome is problematic. Therefore, we identified putative ADAR substrates by isolating the RNAs that coimmunoprecipitate with ADAR. We find that ADAR interacts with mRNAs encoding transcriptional regulators, zinc-finger proteins, and components of the secretory pathway. A similar approach has been taken to identify ADAR substrates in human B cells (Wang et al. 2013), and the results indicate that human ADAR1 also targets mRNAs encoding zinc-finger proteins. It is remarkable that *Xenopus* and human ADAR target similar classes of mRNAs, as the vast majority of A-to-I editing events in the human transcriptome occur in primate-specific Alu elements, which are absent in frogs.

Role of dsRNA length in ADAR-RNP formation

Our data reveal that the length of a dsRNA affects its localization to spindle microtubules in *Xenopus* egg extract. Double-stranded RNAs over 1.5 kbp localize robustly to spindle poles, whereas RNAs with ∼500 bp of double-stranded structure localize poorly or not at all, despite the fact that they can be targeted for editing by ADAR. We hypothesize that the ability to distinguish very long from moderate stretches of dsRNA might allow the cell to differentiate between RNAs derived from viruses or transposable elements and mRNAs with hairpins. In our model, the former are incorporated into microtubule-associated stress granules, whereas the latter are targeted to storage mRNPs that do not interact with microtubules.

The observation that a cell can "measure" the length of a double-stranded RNA has precedent. Two antiviral response proteins, RIG-I and MDA5, have been shown to selectively recognize dsRNAs of different lengths, with RIG-I preferentially recognizing shorter dsRNAs (<1 kbp) and MDA5 preferentially recognizing longer dsRNAs (>1 kbp) (Kato et al. 2008). MDA5's selectivity for long dsRNA is due to its ability to assemble into cooperative filaments along dsRNA. The dissociation of MDA5 filaments from dsRNA decreases as filament length increases, thus promoting accumulation of MDA5 on longer substrates (Peisley et al. 2011). An exciting avenue for future investigations will be to determine which factors in *Xenopus* egg extract are responsible for differentiating between shorter and longer dsRNA. Likewise, it will be interesting to identify which motor or microtubule-binding proteins mediate microtubule localization of the ADAR complexes containing long dsRNA.

Concluding remarks

Our results demonstrate the novel association of ADAR with two distinct RNP complexes in *X. laevis.* Although these two complexes share many protein components, they recruit different RNAs and display disparate localization patterns. Future studies to determine the cellular function of the complexes will likely inform our understanding of the role of A-to-I RNA editing beyond mRNA re-coding.

MATERIALS AND METHODS

Xenopus egg extracts, spindle assembly, RNA-localization assay

Xenopus egg extract was prepared as in Hannak and Heald (2006). Meiotic spindles were assembled by adding sperm nuclei to egg extract at a final concentration of 500 nuclei/μL, then adding $CaCl_2$ to 0.6 mM to cycle extract into interphase for 90 min, and finally rearresting in meiosis with 1 volume of uncycled egg extract (Hannak and Heald 2006). Spindles were allowed to form for 20 min at 20°C. For RNA-localization assays, 1.56 kb single, double, or partially double-stranded RNAs were added to a final concentration of 12.5 nM. (Note: high concentrations of dsRNA impair spindle localization, perhaps because excess dsRNA is a known inhibitor of ADAR [Hough and Bass 1994].) Whether or not RNA was added, the reaction was incubated for an additional 40 min at 20°C. The samples were then diluted in a buffer containing 1× BrB80, 30% glycerol, 0.5% Triton X-100, 4% paraformaldehyde, and 0.1% glutaraldehyde, and meiotic spindles were purified from other cellular components by centrifugation through a glycerol cushion onto coverslips as described (Hannak and Heald 2006). Coverslips were fixed in −20°C methanol for 2 min and processed for immunofluorescence or mounted in Vectashield (Vector Laboratories) with DAPI. Images were acquired with an Olympus BX61 microscope equipped with a charge-coupled device camera (ORCA) using a 60× 1.42NA objective and an Olympus DSU spinning disc confocal. When used, HiLyte Fluor 488- or rhodamine-tubulin (Cytoskeleton, Inc.) was added to the egg extract at a final concentration of 10–20 μg/mL before cycling into interphase.

Spindle pelleting assay

Spindles were formed as described above, diluted in a buffer containing 1× BrB80, 30% glycerol, and 0.5% Triton X-100 and pelleted through a 10 mL cushion of 60% glycerol and 1× Brb80 as described in Blower et al. (2007). For RNA analysis, the pellets were resuspended in TRIzol (Life Technologies). To study coprecipitating proteins, the spindle pellets were resuspended in 1× XB buffer (Hannak and Heald 2006) and analyzed by SDS-PAGE.

In vitro transcribed RNA constructs

The keratin-19 RNA constructs were transcribed from a 1.56 kb fragment of the *X. laevis* keratin-19 cDNA sequence (I.M.A.G.E. clone # 8072827, Dharmacon RNAi and Gene Expression, pMB319). The fragment used begins and ends with the following sequences:

5′-gcaactctaagcctgacacagctg…….gtcttaataaatggtttttgggccaagcat-3′

The Ime1 RNA was transcribed from a 1.5 kb DNA fragment of the *S. cerevisiae* IME1 promotor (pMB587) (Jambhekar and Amon 2008). The fragment used begins and ends with the following sequences:

5′-caaaggggaaacgccaagaac…..caggtaggaacttcccagtgggt-3′

The bysl RNA was transcribed from the 1.75 kb *X. laevis* bysl cDNA (NM_001091589.1, pMB722).

RNAs were in vitro transcribed with T7 RNA polymerase and capped using the ScriptCap m7G capping system (CellScript), except bysl which was transcribed with T3 and T7 RNA polymerases. For fluorescent labeling, in vitro transcription was performed with a ratio of unlabeled CTP to Cy3-labeled CTP (GE Healthcare Life Sciences) of 20:1. Double or partially double-stranded RNAs were annealed at 0.05 μM in a buffer containing 10 mM HEPES, pH 7.7, 1 mM $MgCl_2$, and 100 mM KCl. Samples were heated to 70°C for 10 min, heated to 75°C for 1 min, cooled to 37°C, and then cooled to room temperature. Annealed RNAs were ethanol precipitated and resuspended in deionized water, and proper annealing was verified by native agarose gel electrophoresis.

Antibodies

ADAR antibody gifted by Michael Jantsch was used for preliminary immunofluorescence experiments at a dilution of 1:250. Additional ADAR antibody was generated by Covance against a 6× His-tagged version of the same ADAR peptide used to raise the Jantsch laboratory antibody (pMB520) (Eckmann and Jantsch 1999). This antibody was affinity purified and used at 0.1 μg/mL for immunofluorescence and 0.6–1.0 μg/mL for Western blots. The Staufen1 antibody was generated by Covance against 6× His-tagged *Xenopus laevis* Staufen1. It was affinity purified and used at 0.5 μg/mL for immunofluorescence and 1.0 μg/mL for Western blots. CBTF122 antibody was a gift from Brenda Bass and was used at 1:200 for immunofluorescence and 1:2000 for Western blots. RAP55 and Xp54 antibodies were gifts from John Sommerville. The RAP55 antibody was used at 1:10,000 for Western blots, and the Xp54 antibody was used at 1:1000 for immunofluorescence and 1:10,000 for Western blots. The Vera antibody was a gift from Bruce Schnapp and was used at 1:1000 for immunofluorescence and 1:10,000 for Western blots. The 40S ribosomal protein S6 antibody (Cell Signaling) was used at a concentration of 1:200 for immunofluorescence. The Xiwi antibody (Lau et al. 2009) was used at 2.5 μg/mL for immunofluorescence. The XMAP215 antibody was generated by Covance against the N-terminus of XMAP215, affinity purified, and used at 1:1000 for Western blots. For immunofluorescence assays, the secondary antibody was Alexa 488-conjugated αRabbit IgG (Invitrogen–Molecular Probes) used at 1:1000. For Western blots, the secondary antibody was either HRP-conjugated αRabbit IgG used at 1:10,000 (Jackson ImmunoResearch) or Trueblot αRabbit IgG (eBioscience) used at 1:1000. Mock immunodepletions were performed with ChromPure Rabbit IgG (Jackson ImmunoResearch).

Immunofluorescence

Purified spindles pelleted onto coverslips (as above) were rehydrated in PBS + 0.1% Triton for 5 min, blocked in blocking buffer (PBS, 0.1% Triton, 1% milk) for 15 min and incubated overnight at 4°C with the primary antibody in blocking buffer. Coverslips were washed three times in PBS + 0.1% Triton for 5 min each and incubated 1 h at room temperature with secondary antibody in blocking buffer. Samples were mounted in Vectashield (Vector Laboratories) with DAPI and imaged as above.

RNA degradation assay

A 1.56-kb Cy3-labeled RNA (see above) was added to *Xenopus* egg extract at a final concentration of 12.5 nM. The reaction was incubated at 20°C and samples taken at each time point were flash frozen in liquid nitrogen. RNA was purified from samples using an RNeasy Mini Kit (Qiagen). To maximize denaturation of the purified dsRNA, it was heated to 95°C for 5 min in a buffer containing (20 mM MOPS, pH 7, 2 mM sodium acetate, 1 mM EDTA, 8% formaldehyde, 50% formamaide). Samples were run on a 1.5% formaldehyde agarose gel and viewed on a Typhoon Trio+ (GE Healthcare Life Sciences) imager. Band intensities were quantified using ImageQuant software (GE Healthcare Life Sciences).

Luciferase assay

A 1.56 kb dsRNA was added to egg extract at a final concentration of 12.5 nM. The extract was incubated for 15 min at 20°C. Then, Renilla Luciferase mRNA (in vitro transcribed and capped as described above from a Renilla Luciferase DNA template [Promega]) was added to the egg extract at a final concentration of 10 nM. The extract was incubated for 1 h at 20°C, and luciferase activity was measured using the Dual-Glo Luciferase Assay System (Promega).

Analysis of eIF2α phosphorylation

Mitotic HeLa extract was prepared as described (Gaglio et al. 1997; Chang et al. 2009). Double-stranded Ime1 RNA was incubated in *Xenopus* egg extract at 0, 1, or 10 nM for 1 h at 20°C. Double-stranded Ime1 RNA was incubated in mitotic HeLa extract at 0, 1, or 10 nM for 1 h at 33°C. Samples were analyzed by Western blot for

total eIF2α (Cell Signaling Technologies, 9722S) or eIF2α phosphorylated at Ser51 (Cell Signaling Technologies, 3597S).

RNA editing assay

For the experiment in Figure 2D, dsRNA corresponding to a fragment of the IME1 yeast promotor (described above) was added to egg extract at a final concentration of 12.5 µg/mL. The reaction was incubated for 40 min at 20°C. Following incubation, RNA was isolated using the RNeasy Mini Kit (Qiagen). Isolated RNA was reverse transcribed with an IME1 promotor specific primer, PCR amplified, cloned into pCR2.1-TOPO using the TOPO TA Cloning Kit (Life Technologies), and sequenced. A 300 base region (containing 85 adenosines) was analyzed for A-to-I editing in 10–17 clones for each reaction.

For the experiments in Figure 7, a 26 base sequence was added to the 3′ end of the keratin-19 sense strand to allow for reverse-transcription of the exogenous, but not the endogenous, keratin-19 mRNA. Prior to fixation and pelleting of the spindles in Figure 7A, samples of each reaction were taken for RNA isolation using the RNeasy Mini Kit (Qiagen). Isolated RNA was reverse transcribed with a primer specific to the 3′ end of the exogenous keratin-19 construct, PCR amplified, TOPO cloned (Life Technologies), and sequenced. A 591 base region (containing 207 adenosines) was analyzed for A-to-I editing in five to seven clones for each reaction.

Purification of dsRNA-interacting proteins from *Xenopus* egg extract

An 18 nt RNA oligonucleotide biotinylated at the 5′ end was purchased from Integrated DNA Technologies. The oligonucleotide sequence matched the first 18 bases of the sense strand of our 1.56-kb keratin-19 fragment. The oligonucleotide was annealed to the antisense strand of our keratin-19 RNA fragment to produce the biotinylated ssRNA construct. The dsRNA construct was produced by also annealing the sense strand of the keratin-19 RNA fragment (minus the first 18 bases). Our biotinylated ssRNA and dsRNA constructs were coupled to streptavidin-coated magnetic beads using the Dynabeads KilobaseBINDER Kit (Invitrogen). The RNA-coupled beads were incubated in *Xenopus* egg extract for 90 min at 20°C. The beads were washed with a buffer containing 100 mM HEPES, pH 7.7, 1 mM $MgCl_2$, 100 mM KCl, and 50 mM sucrose. Proteins were eluted in a sample buffer containing 0.2% SDS + 40 mM DTT. Eluted samples were run on a 7% polyacrylamide gel. Bands of interest were excised and identified by tandem mass spectrometry (Taplin Mass Spectrometry Facility, Harvard Medical School).

Immunodepletions

For immunodepletions from *Xenopus* egg extract, antibodies were coupled to Protein A Dynabeads (Life Technologies). Antibody-coupled beads were added to egg extract at the following concentrations (assuming saturation of beads with antibody): 0.25 µg αADAR/µL egg extract, 1.0 µg αStaufen1/µL egg extract, 1.0 µg total rabbit IgG/µL egg extract (Fig. 2A,B), or 0.25 µg total rabbit IgG/µL egg extract (Fig. 2D). Reactions were incubated for 1 h at 4°C or 20°C before the depleted supernatant was recovered.

For the ADAR rescue in Figure 2D, recombinant *X. laevis* ADAR was added to a final concentration of 1 µM. We measure the concentration of endogenous ADAR in *Xenopus* egg extract to be ~360 nM by quantitative Western blot using our recombinant protein as a standard (data not shown).

ADAR immunoprecipitation

αADAR or total rabbit IgG were bound to Protein A Dynabeads (Life Technologies). Except for the experiment in Figure 4B, antibodies were covalently coupled to the Protein A beads using dimethyl pimelimidate. Antibody-coupled beads were added to egg extract at 0.25 µg antibody/µL egg extract (assuming saturation of beads with antibody), and reactions were incubated for 1 h at 4°C or 20°C. Beads were washed with IP Wash Buffer (100 mM HEPES, pH 7.7, 1 mM $MgCl_2$, 100 mM KCl, and 50 mM sucrose), IP Wash Buffer + 1% Triton, and IP Wash Buffer again, with one exception: for construction of the ADAR-precipitated RNA library (Fig. 4B), the second wash contained 0.5% Triton. Samples were eluted in a buffer containing 0.2% SDS + 40 mM DTT. To isolate coprecipitating RNAs, samples were subjected to Proteinase K digestion followed by phenol/chloroform extraction. To identify coprecipitating proteins, samples were run on an 8% polyacrylamide gel and analyzed by silver staining (SilverQuest Silver Staining Kit, Invitrogen) or Western blot. For samples that were RNase treated, RNaseA TypeX IIA (Sigma) was added to egg extract at a final concentration of 0.1 mg/mL and incubated for 30 min at 20°C prior to addition of the antibody-coupled beads.

Protein purification

Xenopus laevis ADAR cDNA was cloned from egg extract. A construct was created encoding an N-terminal Flag tag followed by a shorter isoform of *Xenopus* ADAR (pMB716) (beginning at methionine 364 of the full-length isoform). The shorter protein isoform was used as it runs to the same position as endogenous *Xenopus* ADAR (Brenda Bass, pers. comm. and data not shown) and as evidence exists that full-length ADAR expressed in *Xenopus* oocytes undergoes proteolytic cleavage at the N-terminus (Eckmann and Jantsch 1999). The Flag-ADAR construct was expressed in Sf9 cells using the Bac-to-Bac Baculovirus Expression System (Invitrogen). Sf9 cells were lysed by dounce homogenization in Lysis Buffer (50 mM Tris, pH 7.6, 150 mM NaCl, and 1% TritonX-100) with cOmplete Protease Inhibitor Cocktail Tablets (Roche) added as recommended. Lysate was cleared at 20,000*g* for 15 min, and the cleared lysate was incubated with αFlag M2 Magnetic Agarose Beads (Sigma-Aldrich) that had been equilibrated in Lysis Buffer for 1 h at 4°C. Beads were washed with 10 column volumes of Lysis Buffer, 10 column volumes of Stringent Wash Buffer (50 mM Tris, pH 7.6, 600 mM NaCl, and 1% Triton X-100), 10 column volumes of Lysis Buffer. Protein was eluted with Lysis Buffer + 100 µg/mL Flag Peptide (Sigma-Aldrich). Eluted protein was concentrated using Amicon Ultra Centrifugal Filters (Millipore) and dialyzed into Storage Buffer (20 mM Tris, pH 7.6, 150 mM NaCl, and 10% glycerol).

Full-length Staufen1 and the ADAR protein fragment used to generate αStaufen1 and αADAR antibodies, respectively, were cloned with N-terminal 6× His tags and expressed in *Escherichia coli*. Cells were resuspended in Buffer A (50 mM $NaPO_4$ pH 8,

300 mM NaCl, and 10 mM imidazole) with cOmplete EDTA-Free Protease Inhibitor Cocktail Tablets (Roche) and lysed by French Press. Lysate was cleared at 20,000*g* for 30 min and bound to NiNTA Agarose Resin (Qiagen). Resin was washed in 20 column volumes Buffer A with 20 mM imidazole. Protein was eluted in Buffer A with 250 mM imidazole and dialyzed into PBS.

Library construction

RNAs were isolated from pelleted spindles (as described above) or ADAR immunoprecipitations (as described above). Strand-specific Illumina libraries were prepared using the TruSeq RNA Sample Preparation v2 Kit (Illumina) according to manufacturer's instructions.

Sequencing analysis

Sequencing reads from Illumina Hi-Seq were aligned to a draft version of the *X. laevis* genome (Laevis 7_0, downloaded from Xenbase [xenbase.org]) using TopHat/Cufflinks (Trapnell et al. 2010) or to the NCBI *X. laevis* Unigene database (downloaded in May 2012) using Bowtie (Langmead et al. 2009). To measure gene expression of reads aligned to the *X. laevis* genome we created gene models using Cufflinks. We aligned 16 different mRNA expression libraries generated in our laboratory to the Laevis 7_0 genome and created transcript models de novo using Cufflinks. We then merged these transcript models with the JGI gene models (downloaded from Xenbase). These gene models were further filtered to include only multiexonic genes using the gffread tool from the Cufflinks suite. Relative gene expression of sequencing libraries was quantified using the cuffdiff program and the gene models created as described above. For alignment to Unigene models, reads were collapsed into unique sequences and aligned to the Unigene transcripts allowing for one mismatch. Normalized alignment counts were calculated using a custom Perl script. Only transcripts with >100 normalized alignment counts were included in further analyses. Reads aligned to Unigene were used to compare ADAR enrichment and translational efficiency using the data set from Subtelny et al. (2014) downloaded from GEO.

Analysis of predicted mRNA structure

To predict regions of mRNAs with the potential to form hairpin structures, sequences from transcript models were searched against themselves using BLAT with the parameter minScore = 15. BLAT output was filtered to identify transcripts that matched themselves in a sense/antisense configuration. Several predicted hairpins were analyzed using mFold to confirm that the regions predicted to form hairpins by this analysis folded into predicted dsRNA structures (data not shown).

To predict regions of mRNAs with the potential to form intermolecular dsRNA structures, sequences from transcript models that were expressed at a level of 100 total reads per extract were searched against themselves as described above. BLAT output was filtered to identify transcripts that could pair in *trans* in a sense:antisense manner. For each gene the best possible pair with another mRNA was retained.

To determine if regions in mRNAs that were predicted to form intramolecular or intermolecular dsRNA were the result of repetitive elements, we used BLAT to compare our transcript models to *Xenopus* repetitive sequences in Repbase (Jurka et al. 2005). Repetitive matches to predicted regions of dsRNA are identified in Supplemental Table 1.

Gene ontology

To perform gene ontology using *X. laevis* transcripts, we first mapped transcripts generated by Cufflinks to the Human Uniprot database. We used BlastX to search Cufflinks transcripts against the human Uniprot database and retained all hits with an *e*-value of $<1 \times 10^{-20}$. We then used the human Uniprot accession numbers as input for GO-enrichment analysis using NCBI DAVID (Huang da et al. 2009a,b). The ontology analysis was performed by comparing the ADAR-precipitated RNA library against the total RNA library.

Statistical analysis

P-values were calculated using the "stats" package in R (R_Core_Team 2013).

DATA DEPOSITION

RNA sequences associated with this manuscript have been deposited into the NIH SRA under accession number (BioProject: PRJNA255991).

SUPPLEMENTAL MATERIAL

Supplemental material is available for this article.

ACKNOWLEDGMENTS

We are grateful to Brenda Bass for generously sharing plasmids, antibodies, and knowledge and to Michael Jantsch, John Sommerville, and Bruce Schnapp for kindly providing antibodies. We thank the MGH Sequencing Core for sequencing our Illumina libraries, members of the Blower laboratory for critically reading this manuscript, and Elijah Carrier for help optimizing Western blot conditions. This research was funded with the following grants: National Institutes of Health (NIH) RO1 (RO1GM086434) (M.D.B.), Burroughs Wellcome Fund Career Award in the Biomedical Sciences (M.D.B.), NIH F32 GM090533 (C.T.H.S.), National Science Foundation (NSF) GRFP (A.B.E.).

Received August 19, 2014; accepted November 20, 2014.

REFERENCES

Athanasiadis A, Rich A, Maas S. 2004. Widespread A-to-I RNA editing of Alu-containing mRNAs in the human transcriptome. *PLoS Biol* **2:** e391.

Bartoli KM, Bishop DL, Saunders WS. 2011. The role of molecular microtubule motors and the microtubule cytoskeleton in stress granule dynamics. *Int J Cell Biol* **2011:** 939848.

Bass BL. 2002. RNA editing by adenosine deaminases that act on RNA. *Annu Rev Biochem* **71:** 817–846.

Bass BL, Weintraub H. 1987. A developmentally regulated activity that unwinds RNA duplexes. *Cell* **48:** 607–613.

Bass BL, Weintraub H. 1988. An unwinding activity that covalently modifies its double-stranded RNA substrate. *Cell* **55:** 1089–1098.

Bazak L, Haviv A, Barak M, Jacob-Hirsch J, Deng P, Zhang R, Isaacs FJ, Rechavi G, Li JB, Eisenberg E, et al. 2014. A-to-I RNA editing occurs at over a hundred million genomic sites, located in a majority of human genes. *Genome Res* **24:** 365–376.

Blower MD, Feric E, Weis K, Heald R. 2007. Genome-wide analysis demonstrates conserved localization of messenger RNAs to mitotic microtubules. *J Cell Biol* **179:** 1365–1373.

Borchert GM, Gilmore BL, Spengler RM, Xing Y, Lanier W, Bhattacharya D, Davidson BL. 2009. Adenosine deamination in human transcripts generates novel microRNA binding sites. *Hum Mol Genet* **18:** 4801–4807.

Brzostowski J, Robinson C, Orford R, Elgar S, Scarlett G, Peterkin T, Malartre M, Kneale G, Wormington M, Guille M. 2000. RNA-dependent cytoplasmic anchoring of a transcription factor subunit during *Xenopus* development. *EMBO J* **19:** 3683–3693.

Capshew CR, Dusenbury KL, Hundley HA. 2012. Inverted Alu dsRNA structures do not affect localization but can alter translation efficiency of human mRNAs independent of RNA editing. *Nucleic Acids Res* **40:** 8637–8645.

Chang P, Coughlin M, Mitchison TJ. 2009. Interaction between Poly (ADP-ribose) and NuMA contributes to mitotic spindle pole assembly. *Mol Biol Cell* **20:** 4575–4585.

Chen L, Li Y, Lin CH, Chan TH, Chow RK, Song Y, Liu M, Yuan YF, Fu L, Kong KL, et al. 2013. Recoding RNA editing of AZIN1 predisposes to hepatocellular carcinoma. *Nat Med* **19:** 209–216.

Deshler JO, Highett MI, Schnapp BJ. 1997. Localization of *Xenopus* Vg1 mRNA by Vera protein and the endoplasmic reticulum. *Science* **276:** 1128–1131.

Desterro JM, Keegan LP, Jaffray E, Hay RT, O'Connell MA, Carmo-Fonseca M. 2005. SUMO-1 modification alters ADAR1 editing activity. *Mol Biol Cell* **16:** 5115–5126.

Donnelly N, Gorman AM, Gupta S, Samali A. 2013. The eIF2α kinases: their structures and functions. *Cell Mol Life Sci* **70:** 3493–3511.

Eckmann CR, Jantsch MF. 1999. The RNA-editing enzyme ADAR1 is localized to the nascent ribonucleoprotein matrix on *Xenopus lampbrush* chromosomes but specifically associates with an atypical loop. *J Cell Biol* **144:** 603–615.

Eliscovich C, Peset I, Vernos I, Méndez R. 2008. Spindle-localized CPE-mediated translation controls meiotic chromosome segregation. *Nat Cell Biol* **10:** 858–865.

Ferrandon D, Elphick L, Nüsslein-Volhard C, St Johnston D. 1994. Staufen protein associates with the 3′UTR of bicoid mRNA to form particles that move in a microtubule-dependent manner. *Cell* **79:** 1221–1232.

Ferrandon D, Koch I, Westhof E, Nüsslein-Volhard C. 1997. RNA-RNA interaction is required for the formation of specific bicoid mRNA 3′ UTR-STAUFEN ribonucleoprotein particles. *EMBO J* **16:** 1751–1758.

Gaglio T, Dionne MA, Compton DA. 1997. Mitotic spindle poles are organized by structural and motor proteins in addition to centrosomes. *J Cell Biol* **138:** 1055–1066.

Gerbi SA, Borovjagin AV. 2000. Pre-ribosomal RNA processing in multicellular organisms. In *Madame Curie bioscience database* [Internet]. Landes Bioscience, Austin, TX.

Gray MW. 2012. Evolutionary origin of RNA editing. *Biochemistry* **51:** 5235–5242.

Groisman I, Huang YS, Mendez R, Cao Q, Theurkauf W, Richter JD. 2000. CPEB, maskin, and cyclin B1 mRNA at the mitotic apparatus: implications for local translational control of cell division. *Cell* **103:** 435–447.

Hannak E, Heald R. 2006. Investigating mitotic spindle assembly and function in vitro using *Xenopus laevis* egg extracts. *Nat Protoc* **1:** 2305–2314.

Higuchi M, Maas S, Single FN, Hartner J, Rozov A, Burnashev N, Feldmeyer D, Sprengel R, Seeburg PH. 2000. Point mutation in an AMPA receptor gene rescues lethality in mice deficient in the RNA-editing enzyme ADAR2. *Nature* **406:** 78–81.

Hough RF, Bass BL. 1994. Purification of the *Xenopus laevis* double-stranded RNA adenosine deaminase. *J Biol Chem* **269:** 9933–9939.

Huang da W, Sherman BT, Lempicki RA. 2009a. Bioinformatics enrichment tools: paths toward the comprehensive functional analysis of large gene lists. *Nucleic Acids Res* **37:** 1–13.

Huang da W, Sherman BT, Lempicki RA. 2009b. Systematic and integrative analysis of large gene lists using DAVID bioinformatics resources. *Nat Protoc* **4:** 44–57.

Hundley HA, Bass BL. 2010. ADAR editing in double-stranded UTRs and other noncoding RNA sequences. *Trends Biochem Sci* **35:** 377–383.

Hundley HA, Krauchuk AA, Bass BL. 2008. *C. elegans* and *H. sapiens* mRNAs with edited 3′ UTRs are present on polysomes. *RNA* **14:** 2050–2060.

Ingolia NT, Ghaemmaghami S, Newman JR, Weissman JS. 2009. Genome-wide analysis in vivo of translation with nucleotide resolution using ribosome profiling. *Science* **324:** 218–223.

Jambhekar A, Amon A. 2008. Control of meiosis by respiration. *Curr Biol* **18:** 969–975.

Jambhekar A, Emerman AB, Schweidenback CT, Blower MD. 2014. RNA stimulates Aurora B kinase activity during mitosis. *PLoS One* **9:** e100748.

Jansen RP, Niessing D. 2012. Assembly of mRNA-protein complexes for directional mRNA transport in eukaryotes—an overview. *Curr Protein Pept Sci* **13:** 284–293.

Johnston JA, Ward CL, Kopito RR. 1998. Aggresomes: a cellular response to misfolded proteins. *J Cell Biol* **143:** 1883–1898.

Johnston JA, Illing ME, Kopito RR. 2002. Cytoplasmic dynein/dynactin mediates the assembly of aggresomes. *Cell Motil Cytoskeleton* **53:** 26–38.

Jurka J, Kapitonov VV, Pavlicek A, Klonowski P, Kohany O, Walichiewicz J. 2005. Repbase Update, a database of eukaryotic repetitive elements. *Cytogenet Genome Res* **110:** 462–467.

Kato H, Takeuchi O, Mikamo-Satoh E, Hirai R, Kawai T, Matsushita K, Hiiragi A, Dermody TS, Fujita T, Akira S. 2008. Length-dependent recognition of double-stranded ribonucleic acids by retinoic acid-inducible gene-I and melanoma differentiation-associated gene 5. *J Exp Med* **205:** 1601–1610.

Kim DD, Kim TT, Walsh T, Kobayashi Y, Matise TC, Buyske S, Gabriel A. 2004. Widespread RNA editing of embedded alu elements in the human transcriptome. *Genome Res* **14:** 1719–1725.

Kimelman D, Kirschner MW. 1989. An antisense mRNA directs the covalent modification of the transcript encoding fibroblast growth factor in *Xenopus* oocytes. *Cell* **59:** 687–696.

Kingsley EP, Chan XY, Duan Y, Lambert JD. 2007. Widespread RNA segregation in a spiralian embryo. *Evol Dev* **9:** 527–539.

Knoop V. 2011. When you can't trust the DNA: RNA editing changes transcript sequences. *Cell Mol Life Sci* **68:** 567–586.

Ladomery M, Wade E, Sommerville J. 1997. Xp54, the *Xenopus* homologue of human RNA helicase p54, is an integral component of stored mRNP particles in oocytes. *Nucleic Acids Res* **25:** 965–973.

Lambert JD, Nagy LM. 2002. Asymmetric inheritance of centrosomally localized mRNAs during embryonic cleavages. *Nature* **420:** 682–686.

Langmead B, Trapnell C, Pop M, Salzberg SL. 2009. Ultrafast and memory-efficient alignment of short DNA sequences to the human genome. *Genome Biol* **10:** R25.

Lau NC, Ohsumi T, Borowsky M, Kingston RE, Blower MD. 2009. Systematic and single cell analysis of *Xenopus* Piwi-interacting RNAs and Xiwi. *EMBO J* **28:** 2945–2958.

Lécuyer E, Yoshida H, Parthasarathy N, Alm C, Babak T, Cerovina T, Hughes TR, Tomancak P, Krause HM. 2007. Global analysis of mRNA localization reveals a prominent role in organizing cellular architecture and function. *Cell* **131:** 174–187.

Li JB, Church GM. 2013. Deciphering the functions and regulation of brain-enriched A-to-I RNA editing. *Nat Neurosci* **16:** 1518–1522.

Liang H, Landweber LF. 2007. Hypothesis: RNA editing of microRNA target sites in humans? *RNA* **13:** 463–467.

Lund E, Sheets MD, Imboden SB, Dahlberg JE. 2011. Limiting Ago protein restricts RNAi and microRNA biogenesis during early development in *Xenopus laevis*. *Genes Dev* **25:** 1121–1131.

Macbeth MR, Schubert HL, Vandemark AP, Lingam AT, Hill CP, Bass BL. 2005. Inositol hexakisphosphate is bound in the ADAR2 core and required for RNA editing. *Science* **309:** 1534–1539.

MacDonald PM. 1990. *bicoid* mRNA localization signal: phylogenetic conservation of function and RNA secondary structure. *Development* **110:** 161–171.

Macdonald PM, Struhl G. 1988. *Cis*-acting sequences responsible for anterior localization of *bicoid* mRNA in *Drosophila* embryos. *Nature* **336:** 595–598.

Miyamura Y, Suzuki T, Kono M, Inagaki K, Ito S, Suzuki N, Tomita Y. 2003. Mutations of the RNA-specific adenosine deaminase gene (DSRAD) are involved in dyschromatosis symmetrica hereditaria. *Am J Hum Genet* **73:** 693–699.

Mowry KL. 1996. Complex formation between stage-specific oocyte factors and a *Xenopus* mRNA localization element. *Proc Natl Acad Sci* **93:** 14608–14613.

Newport J, Kirschner M. 1982a. A major developmental transition in early *Xenopus* embryos: I. Characterization and timing of cellular changes at the midblastula stage. *Cell* **30:** 675–686.

Newport J, Kirschner M. 1982b. A major developmental transition in early *Xenopus* embryos: II. Control of the onset of transcription. *Cell* **30:** 687–696.

Ng SK, Weissbach R, Ronson GE, Scadden AD. 2013. Proteins that contain a functional Z-DNA-binding domain localize to cytoplasmic stress granules. *Nucleic Acids Res* **41:** 9786–9799.

Nishikura K. 2010. Functions and regulation of RNA editing by ADAR deaminases. *Annu Rev Biochem* **79:** 321–349.

Nishikura K, Yoo C, Kim U, Murray JM, Estes PA, Cash FE, Liebhaber SA. 1991. Substrate specificity of the dsRNA unwinding/modifying activity. *EMBO J* **10:** 3523–3532.

Park E, Williams B, Wold BJ, Mortazavi A. 2012. RNA editing in the human ENCODE RNA-seq data. *Genome Res* **22:** 1626–1633.

Peisley A, Lin C, Wu B, Orme-Johnson M, Liu M, Walz T, Hur S. 2011. Cooperative assembly and dynamic disassembly of MDA5 filaments for viral dsRNA recognition. *Proc Natl Acad Sci* **108:** 21010–21015.

Peng Z, Cheng Y, Tan BC, Kang L, Tian Z, Zhu Y, Zhang W, Liang Y, Hu X, Tan X, et al. 2012. Comprehensive analysis of RNA-Seq data reveals extensive RNA editing in a human transcriptome. *Nat Biotechnol* **30:** 253–260.

Polson AG, Bass BL. 1994. Preferential selection of adenosines for modification by double-stranded RNA adenosine deaminase. *EMBO J* **13:** 5701–5711.

Rabinowitz JS, Lambert JD. 2010. Spiralian quartet developmental potential is regulated by specific localization elements that mediate asymmetric RNA segregation. *Development* **137:** 4039–4049.

Raff JW, Whitfield WG, Glover DM. 1990. Two distinct mechanisms localise cyclin B transcripts in syncytial *Drosophila* embryos. *Development* **110:** 1249–1261.

Ranjan M, Tafuri SR, Wolffe AP. 1993. Masking mRNA from translation in somatic cells. *Genes Dev* **7:** 1725–1736.

R_Core_Team. 2013. *R: a language and environment for statistical computing*. R Foundation for Statistical Computing, Vienna, Austria.

Rice GI, Kasher PR, Forte GM, Mannion NM, Greenwood SM, Szynkiewicz M, Dickerson JE, Bhaskar SS, Zampini M, Briggs TA, et al. 2012. Mutations in ADAR1 cause Aicardi-Goutieres syndrome associated with a type I interferon signature. *Nat Genet* **44:** 1243–1248.

Rieder LE, Staber CJ, Hoopengardner B, Reenan RA. 2013. Tertiary structural elements determine the extent and specificity of messenger RNA editing. *Nat Commun* **4:** 2232.

Rujano MA, Bosveld F, Salomons FA, Dijk F, van Waarde MA, van der Want JJ, de Vos RA, Brunt ER, Sibon OC, Kampinga HH. 2006. Polarised asymmetric inheritance of accumulated protein damage in higher eukaryotes. *PLoS Biol* **4:** e417.

Saccomanno L, Bass BL. 1999. A minor fraction of basic fibroblast growth factor mRNA is deaminated in *Xenopus* stage VI and matured oocytes. *RNA* **5:** 39–48.

Scadden AD. 2005. The RISC subunit Tudor-SN binds to hyper-edited double-stranded RNA and promotes its cleavage. *Nat Struct Mol Biol* **12:** 489–496.

Scadden AD, Smith CW. 1997. A ribonuclease specific for inosine-containing RNA: a potential role in antiviral defence? *EMBO J* **16:** 2140–2149.

Sharp JA, Plant JJ, Ohsumi TK, Borowsky M, Blower MD. 2011. Functional analysis of the microtubule-interacting transcriptome. *Mol Biol Cell* **22:** 4312–4323.

Slotkin W, Nishikura K. 2013. Adenosine-to-inosine RNA editing and human disease. *Genome Med* **5:** 105.

St Johnston D. 2005. Moving messages: the intracellular localization of mRNAs. *Nat Rev Mol Cell Biol* **6:** 363–375.

Stein P, Zeng F, Pan H, Schultz RM. 2005. Absence of non-specific effects of RNA interference triggered by long double-stranded RNA in mouse oocytes. *Dev Biol* **286:** 464–471.

Subtelny AO, Eichhorn SW, Chen GR, Sive H, Bartel DP. 2014. Poly(A)-tail profiling reveals an embryonic switch in translational control. *Nature* **508:** 66–71.

Tanaka KJ, Ogawa K, Takagi M, Imamoto N, Matsumoto K, Tsujimoto M. 2006. RAP55, a cytoplasmic mRNP component, represses translation in *Xenopus* oocytes. *J Biol Chem* **281:** 40096–40106.

Thomas MG, Loschi M, Desbats MA, Boccaccio GL. 2011. RNA granules: the good, the bad and the ugly. *Cell Signal* **23:** 324–334.

Trapnell C, Williams BA, Pertea G, Mortazavi A, Kwan G, van Baren MJ, Salzberg SL, Wold BJ, Pachter L. 2010. Transcript assembly and quantification by RNA-Seq reveals unannotated transcripts and isoform switching during cell differentiation. *Nat Biotechnol* **28:** 511–515.

Wagner RW, Nishikura K. 1988. Cell cycle expression of RNA duplex unwindase activity in mammalian cells. *Mol Cell Biol* **8:** 770–777.

Wang Q, Miyakoda M, Yang W, Khillan J, Stachura DL, Weiss MJ, Nishikura K. 2004. Stress-induced apoptosis associated with null mutation of ADAR1 RNA editing deaminase gene. *J Biol Chem* **279:** 4952–4961.

Wang IX, So E, Devlin JL, Zhao Y, Wu M, Cheung VG. 2013. ADAR regulates RNA editing, transcript stability, and gene expression. *Cell Rep* **5:** 849–860.

Weissbach R, Scadden AD. 2012. Tudor-SN and ADAR1 are components of cytoplasmic stress granules. *RNA* **18:** 462–471.

Werner A. 2005. Natural antisense transcripts. *RNA Biol* **2:** 53–62.

Wianny F, Zernicka-Goetz M. 2000. Specific interference with gene function by double-stranded RNA in early mouse development. *Nat Cell Biol* **2:** 70–75.

Wulff BE, Sakurai M, Nishikura K. 2011. Elucidating the inosinome: global approaches to adenosine-to-inosine RNA editing. *Nat Rev Genet* **12:** 81–85.

Xu G, Zhang J. 2014. Human coding RNA editing is generally nonadaptive. *Proc Natl Acad Sci* **111:** 3769–3774.

Yang S, Tutton S, Pierce E, Yoon K. 2001. Specific double-stranded RNA interference in undifferentiated mouse embryonic stem cells. *Mol Cell Biol* **21:** 7807–7816.

Yoon YJ, Mowry KL. 2004. *Xenopus* Staufen is a component of a ribonucleoprotein complex containing Vg1 RNA and kinesin. *Development* **131:** 3035–3045.

Zaranek AW, Levanon EY, Zecharia T, Clegg T, Church GM. 2010. A survey of genomic traces reveals a common sequencing error, RNA editing, and DNA editing. *PLoS Genet* **6:** e1000954.

Zhang Z, Carmichael GG. 2001. The fate of dsRNA in the nucleus: a p54 (nrb)-containing complex mediates the nuclear retention of promiscuously A-to-I edited RNAs. *Cell* **106:** 465–475.